HHS Public Access

Author manuscript

J Med Chem. Author manuscript; available in PMC 2020 October 14.

Published in final edited form as:

J Med Chem. 2020 October 08; 63(19): 10855–10878. doi:10.1021/acs.jmedchem.0c00545.

DPAGT1 Inhibitors of Capuramycin Analogues and Their Antimigratory Activities of Solid Tumors

Katsuhiko Mitachi[a], **Rita G. Kansal**[b], **Kirk E. Hevener**[a], **Cody D. Gillman**[c], **Syed M. Hussain**[b], **Hyun Gi Yun**[c], **Gustavo A. Miranda-Carboni**[d], **Evan S. Glazer**[b], **William M. Clemons Jr.**[c], **Michio Kurosu**[a]

[a]Department of Pharmaceutical Sciences, College of Pharmacy, University of Tennessee Health Science Center, 881 Madison Avenue, Memphis, TN 38163, USA

[b]Department of Surgery and Center for Cancer Research, College of Medicine, University of Tennessee Health Science Center, 910 Madison St., Suite 300, Memphis, TN 38163, USA

[c]Division of Chemistry and Chemical Engineering, California Institute of Technology, 1200 E. California Blvd. Pasadena, CA 91125, USA

[d]Department of Medicine, Division of Hematology-Oncology, University of Tennessee Health Science Center, 19 S. Manassas Avenue, Memphis, TN 38163, USA

Abstract

Capuramycin displays narrow spectrum of antibacterial activity by targeting bacterial translocase I (MraY). In our program of development of new *N*-acetylglucosaminephosphotransferase1 (DPAGT1) inhibitor, we have identified that a capuramycin phenoxypiperidinylbenzylamide analogue (CPPB) inhibits DPAGT1 enzyme with an IC_{50} value of 200 nM. Despite a strong DPAGT1 inhibitory activity, CPPB does not show cytotoxicity against normal cells and a series of cancer cell lines. However, CPPB inhibits migrations of several solid cancers including pancreatic cancers that require high DPAGT1 expression in order for tumor progression. DPAGT1 inhibition by CPPB leads to a reduced expression level of Snail, but does not reduce E-cadherin expression level at the IC_{50} (DPAGT1) concentration. CPPB displays a strong synergistic effect with paclitaxel against growth-inhibitory action of a patient-derived pancreatic adenocarcinoma, PD002: paclitaxel (IC_{50} 1.25 μM) inhibits growth of PD002 at 0.0024–0.16 μM in combination with 0.10–2.0 μM of CPPB (IC_{50} 35 μM).

Graphical Abstract

Corresponding Author: Michio Kurosu - Department of Pharmaceutical Sciences, College of Pharmacy, University of Tennessee Health Science Center, 881 Madison Avenue, Memphis, TN 38163, USA; Phone: +1-901-448-1045; Fax: 901-448-6940; mkurosu@uthsc.edu;.

Supporting Information This material is available free of charge via the Internet at http://pubs.acs.org.
NMR spectra of the compounds in the Experimental Section, all assay data, HPLC chromatogram of new compounds, assay procedures, and molecular formula string (CSV)

The authors declare no competing financial interest.

DEDICATION

This article is dedicated to the memory of Dr. Isao Kitagawa, Professor Emeritus of Pharmaceutical sciences at Osaka University, an inspirational scientist.

Artwork

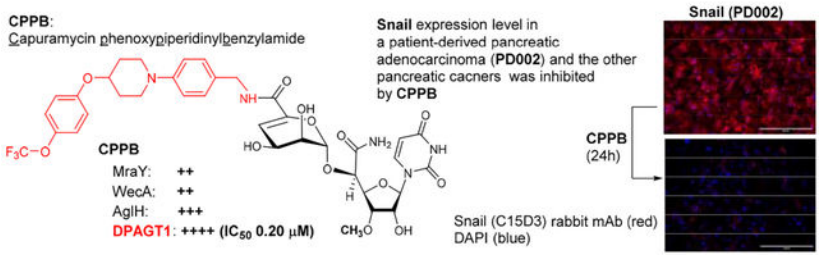

Keywords

Capuramycin analogues; DPAGT1 inhibitor; Antimigratory activity; Snail zinc-finger transcription factors; E-Cadherin; Synergistic effect; Computational chemistry

INTRODUCTION

Capuramycin (CAP (**1**), Figure 1) is a nucleoside antibiotic, which has a narrow-spectrum of activity against Gram-positive bacteria including *Mycobacterium tuberculosis* (Mtb).[1–3] To date, medicinal chemistry efforts on capuramycin have been focused on developing a new TB drug; new capuramycin analogues have been synthesized to improve bacterial phospho-MurNAc-pentapeptide translocase I (MraY and MurX for *Mycobacterium* spp.) enzyme as well as antimycobacterial activities.[1,4,5] Somewhat recently, the anti-*Clostridioides difficile* (formerly *Clostridium difficile*) activity of a capuramycin analogue has been reported.[6] Capuramycin is a specific inhibitor of MraY with the IC_{50} value of 0.13 μM,[7] however, some other nucleoside antibiotics (*e.g.*, muraymycin A1 and tunicamycins) display activity against MraY, WecA (polyprenyl phosphate-GlcNAc-1-phosphate transferase), and its human homologue, DPAGT1 (*N*-acetylglucosaminephosphotransferase1)-type phosphotransferases.[8–14] MraY is an essential enzyme for growth of the vast majority of bacteria that catalyzes the transformation from UDP-MurNAc-pentapeptide (Park's nucleotide) to prenyl-MurNAc-pentapeptide (lipid I).[15] WecA catalyzes the transformation from UDP-GlcNAc to decaprenyl-P-P-GlcNAc, the first membrane-anchored glycophospholipid that is responsible for the biosynthesis of mycolylarabinogalactan in *Mycobacterium tuberculosis* (Mtb). WecA is an essential enzyme for the growth of Mtb and some other bacteria. Biochemical studies of WecA enzyme are hampered by lack of selective inhibitor molecules.[9] Tunicamycin shows inhibitory activity against these phosphotransferases with the IC_{50} values of 2.9 μM (MraY/MurX), 0.15 μM (WecA), and 1.5 μM (DPAGT1).[9,10] CPZEN-45, an antimycobacterial MraY inhibitor, was reported to exhibit WecA inhibitory activity (IC_{50} ~0.084 μM).[16] We showed that 2'*O*-methyl capuramycin (OM-CAP (**2**), formerly UT-01320, Figure 1) does not exhibit MraY/MurX inhibitory activity, but displays a strong WecA inhibitory activity (IC_{50} 0.060 μM).[1,9] *In vitro* cytotoxicity of tunicamycin has been documented in a number of articles.[17] Acute toxicity of tunicamycin due to its narrow therapeutic window (LD_{50}: 2.0 mg/kg, LD_{100}: 3.5 mg/kg mice, IP) discourages scientists from developing tunicamycin for new antibacterial,

antifungal, or anti-cancer agents.[18,19] A large number of scientists believe that cytotoxicity of tunicamycin is attributable to its interaction with DPAGT1, which catalyzes the first and rate limiting step in the dolichol-linked oligosaccharide pathway in *N*-linked glycoprotein biosynthesis (Figure 2).[10,12] In contrast, OM-CAP (**2**) possesses the same level of DPAGT1 inhibitory activity (IC_{50} 4.5 μM) to tunicamycins (IC_{50} 1.5 μM), but it does not show cytotoxicity against healthy cells (*e.g.*, Vero and HPNE cells) at 50 μM and some cancer cell lines (*e.g.*, L1210, KB, AsPC-1, PANC-1, LoVo, SK-OV-3) at 10 μM. A sharp difference in the cytotoxicity profiles between tunicamycins (**11**, Figure 1) and OM-CAP (**2**) raises the question of whether selective inhibition of DPAGT1 enzyme function in certain cells/organs by small molecules does not cause unacceptable level of toxicity against human during chemotherapy. We have recently engineered the structure of muraymycin to yield strong DPAGT1 inhibitors; one of these analogues, APPB (**12**, Figure 1), showed a promising antiproliferative effect on a series of solid cancer cell lines that required overexpression of the *DPAGT1* gene in their growth and cancer progression.[11,13,14] The design of APPB was originated from the discovery of DPAGT1 inhibitors of capuramycin analogues. In this article, we report structure-activity relationship (SAR) studies of capuramycin to identify novel DPAGT1 inhibitors, and *in vitro* anti-invasion and anti-metastasis activity of a new capuramycin analogue DPAGT1 inhibitor, CPPB (capuramycin phenoxypiperidinylbenzylamide analogue, **5**) (Figure 1). A unique synergistic effect was observed against a patient-derived pancreatic adenocarcinoma, PD002 in a combination of CPPB with paclitaxel. We demonstrated key interactions of CPPB with DPAGT1 via molecular docking studies. Lastly, we report a semi-synthetic method to deliver enough CPPB for future *in vivo* studies.

RESULTS AND DISCUSSION

Chemistry and Structure activity relationship (SAR).

Sankyo (currently Daiichi-Sankyo) and Sequella have reported several capuramycin (CAP, **1**) analogues that have improved MraY enzyme and bacterial growth inhibitory activities.[2,3,5,20] Their SAR studies rely on a capuramycin biosynthetic intermediate, A-500359E, which allows delivery of novel amide molecules (R_1 group) having an ester (R_2) functional group (Figure 3). The capuramycin analogue, SQ992, has an interesting antibacterial characteristic with antimycobacterial activity *in vivo*.[21] We have accomplished a total chemical synthesis of capuramycin and its analogues.[22,] To date, we have identified an novel analogue possessing improved MraY inhibitory activity, Cap-3-amino-1,4-benzodiazepine-2-one analogue,[23] and a selective WecA inhibitor, OM-Cap (**2**), via our total synthetic approach (Figure 3).[1,9] Since our first report on a total synthesis of capuramycin, a few improvements of the synthetic scheme have been made: we introduced acid-cleavable protecting groups for the uridine ureido nitrogen (3-postion in **a**) and primary alcohol (6”-position in **c**) (Scheme 1).[23] The MDPM and MTPM groups can simultaneously be removed with 30% TFA to form the key synthetic intermediate **A** for capuramycin. In our on-going SAR of capuramycin, commercially available protecting groups (BOM and chloroacetyl groups) for the ureido nitrogen (3-position) and C6“-alcohol were decided to apply in our SAR tactics. Success of hydrogenolytic cleavage of the BOM group and tolerability of the chloroacetyl group were difficult to predict in capuramycin synthesis. To establish the new

protecting group strategy, we first demonstrated the synthesis of *iso*-capuramycin (I-Cap) (Scheme 2A). Syntheses of all building blocks and the experimental procedures for their synthetic steps in Scheme 2 and 3 are summarized in Supporting Information (SI). Highlights of syntheses of new capuramycin analogues are illustrated in Scheme 2 and 3. The (*S*)-cyanohydrin **13** was subjected to NIS-$AgBF_4$ promoted α-selective mannosylation with the thioglycoside **14** to yield the α-mannosylated cyanohydrin **15** in 78% yield.[22] The cyano group of **15** was hydrated using $HgCl_2$-aldoxime in aq. EtOH, and the BOM and chloroacetyl groups of the generated amide were deprotected stepwisely: dechloroacetylation with thiourea followed by hydrogenation with 10% Pd-C in AcOH-^{i}PrOH-THF provided the C6”-free alcohol **16** in 53% overall yield. Oxidation-elimination reaction of **16** with SO_3•pyridine in a solvent system (CH_2Cl_2/Et_3N/DMSO = 10/2/1) provided the α, β unsaturated aldehyde **17** in quantitative yield (determined by ^{1}H NMR analysis). After all volatiles were removed, the aldehyde **17** was oxidized to the corresponding carboxylic acid **18** by using $NaClO_2$ in the presence of NaH_2PO_4 and 2-methyl-2-butene.[24] The resulting carboxylic acid **18** was coupled with (*2S*)-aminocaprolactam by using a standard peptide-forming reaction condition (HOBt, EDCI, and NMM) to yield the coupling product **19** in 70% overall yield from **16**. Saponification of **19** by using Et_3N in MeOH provided I-Cap (**3**) in quantitative yield. Similarly, dimethyl-capuramycin (DM-CAP) was synthesized in 31% overall yield from the cyanohydrin-acetonide **20**. CAP (**1**) and its three analogues, OM-CAP (**2**), I-CAP (**3**), and DM-CAP (**4**) were evaluated in enzyme inhibitory assays against bacterial phosphotransferases, MraY and WecA, and archaeal and human dolichyl-phosphate GlcNAc-1-phosphotransferases, AglH and DPAGT1.[7,9,11] CAP is a selective MraY inhibitor that does not display inhibitory activity against WecA, AglH, and DPAGT1 (Table 1). Previously, OM-CAP (**2**) was identified as a selective WecA inhibitor (IC_{50} 0.060 μM) that does not possess MraY inhibitory activity (IC_{50} >50 μM (entry 2 in Table 1).[9] In this program, it was realized that OM-CAP (**2**) has inhibitory activity against AglH and DPAGT1 with the IC_{50} values of 2.5 and 4.5 μM, respectively (entry 2). I-CAP (**3**) showed enzyme inhibitory activity against MraY, WecA, AglH, and DPAGT1 with the IC_{50} between 8.5–30 μM concentrations (entry 3). On the contrary, DM-CAP (**4**) showed only a weak WecA inhibitory activity (IC_{50} 35.0 μM) (entry 4). In recent reports on co-crystal structures of DAPGT1 with tunicamycin (PDB: 5O5E and 6BW6), the fatty acid chain of tunicamycin is occupied in the hydrophobic tunnel (the proposed dolichol-phosphate (Dol-P) binding site).[25,26] We speculated that introduction of pharmacologically amenable hydrophobic groups that occupy the proposed Dol-P binding site is essential to exhibit strong DPAGT1 inhibitory activity. In virtual screening of a hydrophobic group (excluding fatty acids) using the structure of DPAGT1 with bound tunicamycin (PDB: 6BW6), an analogue (*e.g.*, (((trifluoromethoxy)phenoxy)piperidinyl)benzylamide) of (((trifluoromethoxy)phenoxy)piperidin-1-yl)phenol group (*i.e.* **34** in Scheme 3) found in a new anti-TB drug, delamanid,[27,28] was suggested to be a reasonable fatty acid surrogate, whose capuramycin derivatives (capuramycin phenoxypiperidinylbenzylamide (CPPB, **5**), *iso*-capuramycin phenoxypiperidinylbenzylamide (I-CPPB, **6**), *O*-methyl capuramycin phenoxypiperidinylbenzylamide (OM-CPPB, **7**), demethyl capuramycin phenoxypiperidinylbenzylamide (DM-CPPB, **8**), capuramycin phenoxypiperidinylbenzylamine (CPPA, **9**), and *iso*-capuramycin

phenoxypiperidinylbenzylamine (I-CPPA, **10**)) could bind to DPAGT1 with high affinity. However, the docking program used in these studies is not able to distinguish between low- and high-binding molecules: all (((trifluoromethoxy)phenoxy)piperidin-1-yl)phenyl)methanamino derivatives provided "good" GlideScores of between -12.9~-16.6 (see Table S1 in SI). Therefore, we decided to synthesize all analogues (CPPB, I-CPPB, OM-CPPB, DM-CPPB, CPPA, and I-CPPA) identified in the virtual screening and evaluate their phosphotransferase inhibitory activity.

The carboxylic acid intermediate **32** for CAP (**1**) was subjected to peptide coupling reaction with (((trifluoromethoxy)phenoxy)piperidin-1-yl)phenyl)methylamine (**34**), providing the protected CPPB, **37**. Saponification of **37** and purification by reverse HPLC yielded CPPB (**5**) in 95% overall yield from **37**. Similarly, I-CPPB (**6**), OM-CPPB (**7**), and DM-CPPB (**8**) were synthesized from the mannuronic acid derivatives **18**, **33**, and **31** in 24–34% overall yield (Scheme 3A). Capuramycin phenoxypiperidinylbenzylamine analogues, CPPA (**9**) and I-CPPA (**10**), were synthesized via reductive aminations of the aldehydes **29** and **17** with the amine **34**, furnishing the desired products in 63–65% overall yield from **26** and **16** after saponification. MraY, WecA, AglH, and DPAGT1 enzyme inhibitory activity assays for the six (((trifluoromethoxy)phenoxy)piperidin-1-yl)phenyl)methylamine analogues revealed that CPPB (**5**) and I-CPPB (**6**) are high nM range DPAGT1 inhibitors (entries 5 and 6 in Table 1), however, the *O*-methylation and demethylation analogues (OM-CPPB (**7**) and DM-CPPB (**8**)) turned out to be very low- or no-DPAGT1 inhibitor (entries 7 and 8). The secondary amine analogues, CPPA (**9**) and I-CPPA (**10**), did not inhibit all phosphotransferases tested in Table 1 at 50 μM concentration (entries 9 and 10). CPPB was determined to be three times stronger DAPGT1 inhibitor (IC_{50} 0.20 μM) than I-CPPB (entry 5 vs. 6). I-CPPB did not display MraY inhibitory activity, but showed a very weak WecA and AglH enzyme inhibitory activity (entry 6). Interestingly, difference in these phosphotransferase inhibitory profiles between CPPB and I-CPPB correlate with their antimycobacterial activity: CPPB possessing MraY/WecA inhibitory activity killed *Myocobacterium tuberculosis* H_{37}Rv, *Mycobacterium avium* 2285, *Mycobacterium smegmatis* (ATCC607) with the MIC values 6.25–12.5 μg/mL. In contrast, I-CPPB, which does not have MraY inhibitory activity, did not show growth inhibitory activity against these *Mycobacterium* spp. at 50 μg/mL.

Cytotoxicity of new capuramycin analogues, CPPB (5) and I-CPPB (6).

In the capuramycin analogue series, the degree of MraY inhibitory activity correlates with their antimycobaterial activity.[7–9,13] Antimycobacterial capuramycin analogues display low *in vitro* cytotoxicity against mammalian cells, and have been recognized as safe drug leads that have acceptable tolerability in animal models.[2,3] The toxicity of tunicamycin (**11**, Figure 1) has been studied extensively *in vitro*: tunicamycin inhibits growth in many cancer cell lines without selectivity, and has a narrow therapeutic window demonstrated in *in vivo* studies using mice.[18,29] The toxicity of tunicamycin is believed to be attributable to its ability to inhibit DPAGT1 enzyme function.[10,30] However, in our studies, tunicamycin's toxicity could not be explained solely by its inhibition of DPAGT1. Our DPAGT1 inhibitor, APPB (**12**, Figure 1) inhibits DPAGT1 with greater than 30-times the inhibitory activity of tunicamycin, and inhibits growth of selected solid cancer cell lines at low μM concentrations with selective cytotoxicity (IC_{50} normal cells / cancer cells) of >35.[10] The LD_{50} value of

APPB is >20 mg/kg (mouse), whereas it is 2.0 mg/kg (mouse) for tunicamycin.[10,18] Capuramycin-based DPAGT1 inhibitors, CPPB (**5**) and I-CPPB (**6**), identified in this program inhibited DPAGT1 enzyme with the IC_{50} values of 0.2 and 0.6 μM, respectively. Unlike the MraY-antimycobacterial activity relationship observed for CAP analogues, the DPAGT1 inhibitors, CPPB and I-CPPB, did not show antiproliferative activity against L1210 (a leukemia cell), HPNE (a normal pancreatic ductal cell), and Vero (a normal kidney cell) at 50 μM. They showed various levels of growth inhibitory activity against several solid cancer cell lines such as KB (HeLa, a cervix carcinoma), SiHa (a cervical squamous cell carcinoma), HCT-116 (a colorectal adenocarcinoma), DLP-1 (a colorectal adenocarcinoma), Capan-1 (a pancreatic ductal adenocarcinoma), PANC-1 (a pancreatic ductal carcinoma), AsPC-1 (a pancreatic adenocarcinoma), PD002 (a patient-derived pancreatic adenocarcinoma) in MTT assays (IC_{50} 15–45 μM, Table 2). A lower DPAGT1 inhibitor, tunicamycin (**11**), showed growth inhibition of all cell lines in Table 2 with the IC_{50} values of 0.78–7.5 μM concentrations (entry 5 in Table 2). Cellular behavior and morphological changes of a patient-derived metastatic pancreatic adenocarcinoma, PD002 treated with CPPB were monitored over time via IncuCyte® live cell analysis imaging system (Figure 4A). Interestingly, 10–13% of phase area confluent of PD002 culture (time 0h) remained the same after 72h for the CPPB-treated cells (50 μM), whereas, ca. 70% of confluence was reached for the control PD002 culture (PBS) (Figure 4B vs.4C). Although morphological changes were subtle over time (0–72h), cell viability assessed by the MTT reduction assay revealed that PD002 cells treated with CPPB (50 μM) was significantly decreased (Table 2). Exposure of CPPB (0.2–20 μM) inhibited cell proliferation of PD002: ca. 20% of cell proliferation was inhibited at time 72h. These results may indicate that DPAGT1 inhibitors may have cytostatic effect again certain cancerous tumors that require DPAGT1 overexpression for their growth.

Cell migratory inhibition by CPPB (5).

DPAGT1 catalyzes the first step in *N*-glycan biosynthesis of mammalian cells (Figure 2). Aberrant *N*-glycosylation is common in many solid cancers and important for the epithelial to mesenchymal transition program (EMT, a mechanism of metastases).[10] We found high levels of DPAGT1 protein expression in a series of pancreatic cancers (*e.g.*, PANC-1, Capan-1, and AsPC-1). Dysregulation of DPAGT1 enzyme leads to disturbances in cell-cell adhesions and may increase epithelial to mesenchymal transition (EMT): these processes increase migratory and invasive capabilities of malignant neoplasms that are the initiation of metastasis in cancer progression, especially pancreatic cancer.[31,32] Interestingly, there is significant crosstalk between DPAGT1 and the Wnt/β-catenin and Snail pathway where DPAGT1 overexpression leads to 1) accumulation of β-catenin in the cytoplasm and then translocation into the nucleus, and 2) reduction of the Snail expression levels, preventing epithelial-mesenchymal transition by suppressing the E-cadherin expression (a cell-cell adhesion glycoprotein).[10,31,32] As such, aberrations in these pathways occur in numerous cancers, thus, discovery of small molecules directed towards inhibition of the Wnt and Snail pathways represents an important area of anticancer therapeutics.[33–35] In order to obtain insights into anti-metastatic ability of DPAGT1 inhibitors, we explored the degree of cell migration in several commercially available cell lines (Capan-1, PANC-1, and AsPC-1), a patient-derived pancreatic ductal adenocarcinoma cell line (PD002), a cervical carcinoma

(SiHa), and a colorectal adenocarcinoma (HCT-116) to determine the effects on cellular motility. After 24h of three treatment doses (0.05, 0.1, and 0.2 μM) with CPPB (**5**), inhibition of migration (closing the gap) was measured in a scratch assay (wound healing assay).[36] Only the images for PD002 are shown in Figure 5 and all other images obtained through these experiments are illustrated in Supporting Information (SI). The pancreatic cancer cell lines treated with CPPB migrated far less than the PBS treated (control) cells (Figure 5A–D). In these assays, the wound-healing rate of the untreated PD002 cells was 63% in 24h. In sharp contrast, CPPB treated cells inhibited the wound-healing effectively at its IC_{50} level against DPAGT1 (0.2 μM): the wound-healing rate was approximately 20% (Figure 5B). We thoroughly evaluated migration inhibition ability of CPPB compared to gemcitabine, one of the main chemotherapy drugs used to treat pancreatic cancer, and tunicamycin using PD002 cells. Gemcitabine shows a wound-healing rate of 43% at 0.2 μM, and tunicamycin shows 35% at 0.2 μM (SI). Thus, it was concluded that CPPB is more effective in inhibiting cancer cell migration than gemcitabine and tunicamycin. These trends were further confirmed by an endpoint migration assays via Boyden chambers for PD002.[37,38] In these assays, the cell migrations of PD002 treated with CPPB (0.1 μM) were inhibited on a higher level compared to those with tunicamycin and gemcitabine at the same concentration (0.1 μM) (Figure 6).

Inhibition of a zinc-finger transcription factor, Snail1 (Snail) in the selected cancer cell lines by CPPB.

Snail protein is one of the most important transcription factor that induces epithelial to mesenchymal transition (EMT), which converts epithelial cells into migratory mesenchymal cells that are more efficient at metastasizing.[39] EMT induced by overexpression of Snail produces cancer stem-like properties in a number of solid organ cancers. Aberrant expression of Snail leads to loss of expression of E-cadherin.[40] Thus, suppression of Snail expression or inhibition of Snail functions represents a potent targeted therapeutic strategy for many cancers.[41,42]

Immunofluorescence assays using an anti-Snail antibody revealed that the fluorescence intensity of Snail was strong in a series of pancreatic cancer cells (PANC-1, AsPC-1, Capan-1, and PD002), and the expression of Snail was decreased by the treatment with CPPB in a concentration dependent manner. Among pancreatic cancer cell lines, only the data for PD002 and PANC-1 are shown in Figure 7A and 7B (see SI for AsPC-1 and Capan-1). The Snail expression level of a non-metastatic pancreatic cancer, PANC-1, was much lower than metastatic pancreatic cancers (*e.g.*, PD002 and Capan-1). A few other types of cancer cells such as a colorectal cancer (HCT-116) and a cervical cancer (SiHa) were examined by similarly designed immunofluorescence assays or Western blot assays (Figures 7C and 7D). The Snail expression in SiHa was inhibited by treatment of CPPB in a concentration dependent manner; at the IC_{50} concentration (0.2 μM against DPAGT1), CPPB effectively inhibited the Snail expression (Figure 7D). In contrast, the Snail expression level in HCT-116 was not noticeably changed by the treatment of CPPB between 0.05 and 2.0 μM concentrations. Interestingly, cell migration of HCT-116 was not inhibited by CPPB demonstrated in the wound healing (scratch) assays (Figure 5F). At the concentrations tested in the scratch assays (0.05–2.0 μM), the E-Cadherin expression levels

of PD002, PANC-1, and HCT-116 were not changed significantly (Figure 8). To support the above discussion based on the immunefluorescent staining (Figure 7 and 8), the relative expression levels of Snail and E-cadherin in PD002, PANC-1, and HCT-116 treated with CPPB were measured by Western blot analyses (Figure 9). The relative expression levels were obtained by using Image Studio™ Lite quantification software, and these quantified data were summarized in SI (see Figure S5). PD002 and PANC-1 treated with CPPB (0 to 2.0 μM) lead to a dose dependent decrease in Snail. The E-Cadherin expression level of a metastatic pancreatic cancer, PD002 was increased in a CPPB concentration depended manner (0 to 2.0 μM), whereas, a non-metastatic pancreatic cancer, PANC-1 exhibited the same expression level of E-Cadherin at 0–2.0 μM concentrations of CPPB (Figure 9A and 9B). A low DPAGT1 expressed-colon cancer, HCT-116 did not display noticeable difference in the expression levels of Snail and E-Cadherin at 0–2.0 μM CPPB concentrations (Figure 9C).

Inhibition of DPAGT1 by CPPB.

CPPB decreased the DPAGT1 expression level in all pancreatic cancer cell lines examined in Figure 5: the DPAGT1 expression was apparently inhibited by the IC_{50} concentration of CPPB (0.2 μM) (only the data for PD002 and PANC-1 shown Figure 10 and see Figure S4 in SI) for AsPC-1 and Capan-1). An important observation is that the DPAGT1 expression of the pancreatic cancer cell lines could not completely be inhibited at a high concentration of CPPB (2–20 μM) (Figures 9 and 10). In MTT assays, we realized that all pancreatic cancers tested remained viable at 20 μM concentration of CPPB (Table 2). We confirmed that the DPAGT1 expression level in a colorectal adenocarcinoma, HCT-116 is significantly lower than that in the pancreatic cancer cell lines (PD002 and PANC-1); DPAGT1 was not detectable in Western blot assays for the lysate obtained by a standard protocol (50 μg/30 μL of total protein sample). A 10 times concentrated HCT-116 cell lysate (prepared by ultracentrifugation, 130,000xg for 1h) enabled us to detect DPAGT1 in Western blotting. By treatment of HCT-116 with CPPB at 0.1–20 μM concentration, the DPAGT1 expression levels of HCT-116 remained higher fluorescence intensity in immunefluorescent assay (Figure 10C) and 20–90% in Western blot assays (Figure 9C). These data imply that the inhibitory effect of CPPB on cell migration varies depending on degree of inhibition of the DPAGT1 expression: immunefluorescent assays at 0.2–2.0 μM concentrations of CPPB, the degree of DPAGT1 expression was decreased by the following order: PANC-1 > PD002 >> HCT-116. Migration inhibition observed in the scratched assays (Figure 5) is well-correlated with the degree of the DPAGT1 expression inhibition. Although CPPB decreased the protein expression of DPAGT1 without significantly decreasing its gene (*DPAGT1*) expression, tunicamycin decreased both the gene expression of *DPAGT1* and DPAGT1 protein expression (Figure 11). These down-regulation in *DPAGT1* gene expression by tunicamycin may be attributable to its high cytotoxicity against mammalian cells without selectivity.

Synergistic effect of CPPB with paclitaxel.

The FOLFIRINOX (a combination of folinic acid, 5-fluorouracil, irinotecan, and oxaliplatin) and nab-paclitaxel (albumin-bound paclitaxel)-gemcitabine regimens have been adopted into clinical practice for patients with metastatic pancreatic cancers.[43] Median progression-free survival was reported in one study of patients with metastatic pancreatic

cancer to be 6.4 months in the FOLFIRINOX group and 3.3 months in the gemcitabine group.[43,44] Over the past years, the clinical data have not supported that FOLFIRINOX is associated with any better (or worse) survival rates compared to the nab-paclitaxel-gemcitabine regimen as there have been no head-to-head trials.[45] However, the inclusion of paclitaxel and its derivatives in combination regimens remains an important therapeutic strategy in pancreatic cancer chemotherapy since nab-paclitaxel-gemcitabine is associated with less adverse effects (toxicity in patients) than FOLFIRINOX.[46] In this regard, we were very interested in synergistic or additive effects of DPAGT1 inhibitor in combination with paclitaxel. The synergistic or antagonistic activities of CPPB were assessed *in vitro* via checkerboard technique.[47,48] In these experiments, CPPB displayed strong synergistic effects with paclitaxel in a wide range of concentrations against PD002. Table 3 summarizes the results of FIC index analyses for selected combinations of CPPB (IC_{50} 35.0 μM) plus paclitaxel (IC_{50} 1.25 μM) that showed synergistic combination (ΣFIC<0.5). The FIC index below 0.50 was observed for 20 combinations of two molecules out of 96 different concentrations (see Figure S6 in SI). The IC_{50} value of paclitaxel against PD002 was lowered (0.024–0.61 μM) in combination with CPPB (0.1–2.0 μM).

Interaction of CPPB with DPAGT1 (Modeling Studies).

DPAGT1 encompasses ten transmembrane segments, three loops on the ER (endoplasmic reticulum) side, and five loops on the cytoplasmic side. Four loops (CL-1, CL-5, CL-7, and CL-9) on the cytoplasmic side form the UDP-GlcNAc-binding domain.[25,26] The hydrophobic tunnel created by the transmembrane segments (TM-4, TM-5 and CL-9) within the lipid bilayer is predicted to interact with dolychol-phosphate (Dol-P). The weak DPAGT1 inhibitors, *O*-methyl capuramycin (OM-CAP) and *iso*-capuramycin (I-CAP) (Table 1), yielded low docking scores (Glide Scores) using Schrödinger's Glide program: the score for OM-CAP was -12.4 and for I-CAP was -10.9. These scores predicted that OM-CAP and I-CAP possess significantly lower affinity for DPAGT1 than CPPB, which showed a docking score of -16.6 (see Table S1 in SI).[49–51] The docked CPPB-DPAGT1 structure illustrated in Figure 12 shows several key interactions. The C2'-OH acts as a donor in a hydrogen bond to the Glu56 carboxylate. This interaction is likely be lost when the C2'-OH is methylated. Pi-stacking interactions are observed between 1) Phe249 and the uracil ring, and 2) Trp122 and the trifluoromethoxybenzene in the hydrophobic moiety. Asn185 and Ash252 (protonated Asp) form hydrogen-bond(s) to the primary amide and the dihydropyran-hydroxy (C3"-OH) group, respectively. Additional hydrogen-bonds between the uridine ureido group and the backbone amides (Gln44 and Leu46) strengthen the ligand interaction. In this program, capuramycin (CAP), a strong MraY inhibitor with no DPAGT1 inhibitory activity, was successfully engineered to be a relatively strong DPAGT1 inhibitor by introducing a hydrophobic functional group, (((trifluoromethoxy)phenoxy) piperidin-1-yl)phenyl)methylamine at the C6"-position. This hydrophobic group allows the preferable conformation of the uridine-enopyranosiduronic moiety in the DPAGT1 biding domain, resulting in increased interactions with Asn185, Ash252, Glu56, and Phe249.

A semi-synthesis of CPPB from A500359F.

Pharmacological studies of CPPB (**5**) and its related analogues using appropriate animal models will be a focus of our future research efforts. Previously, a natural product

A-5003659E was used to develop novel capuramycin analogues with strong MraY inhibitory activity (Hotoda et. al. 2003) (Figure 3).[52] Its free-carboxylic acid analogue, A-500359F was also isolated from the capuramycin-producing strain, *Streptomyces griseus* Sank 60196. Saponification of A-5003659E to A-500359F was established by the Sankyo group.[20] Although, the currently available synthetic schemes for capuramycin analogues (*e.g.*, Scheme 3) include a relatively short number of chemical steps,[22,23,53] a semi-synthetic approach is more feasible to deliver a large quantities of CPPB for pharmacological studies. To establish semi-synthesis of CPPB, A-500359F was first synthesized from the CAP-synthetic intermediate **32** (Scheme 3A) in a single step. Amide-forming reaction of synthetic A-500359F with (((trifluoromethoxy)phenoxy) piperidin-1-yl)phenyl)methylamine (**34**) was performed under an optimized condition using EDCI, glyceroacetonide-Oxyma, and NMM in DMF.[54] All coupling reagents could be removed by partitions between $CHCl_3$ and water and evaporation. The crude product was passed through DOWEX 50Wx4 column (MeOH : NH_4OH = 4 : 1) to provide CPPB with >95% purity, which was further purified by C_{18}-reverse HPLC (MeOH : H_2O = 65 : 35) to yield pure CPPB (Scheme 4).

CONCLUSION

This paper describes the identification of a new DPAGT1 inhibitor of capuramycin analogue, capuramycin phenoxypiperidinylbenzylamide (CPPB, **5**) and its isostere I-CPPB (**6**). Previously, tunicamycin is the only DPAGT1 inhibitor that has been widely applied to the studies associated with protein misfolding *in vitro*.[55,56] Tunicamycin displays cytotoxicity against cancer and healthy cells with low selectivity ratio.[10] One of cytotoxicity mechanisms of tunicamycin is believed to be its ability to inhibit DPAGT1 enzyme functions. The DPAGT1 expression levels vary depending on the cell types; renal cancers and lymphomas express low-levels of DPAGT1, whereas, a majority of solid cancers express high-levels.[57] Thus, the observed antiproliferative activity of tunicamycin against all types of cancer cells are difficult to understand solely by its DPAGT1 inhibitory activity. In our studies, CPPB showed ~7.5 times stronger DPAGT1 inhibitory activity than tunicamycin. However, unlike tunicamycin, CPPB did not inhibit growth of cancer cell lines at the IC_{50} values observed for tunicamycin (0.45 –7.5 μM). CPPB is a cell-permeable molecule which was demonstrated by IncuCyte® live cell analyses and immunofluorescence assays. In this article, we have studied effectiveness of CPPB on the expression levels of Snail, E-cadherin, and DPAGT1 primary in pancreatic cancers (Figures 7–10). CPPB decreased the Snail expression in commercially available pancreatic cancer cell lines (PANC-1, AsPC-1, and Capan-1) and a patient-derived pancreatic ductal adenocarcinoma cell line (PD002) in a dose dependent manner. On the other hand, the E-cadherin expression level was increased in PD002 (a metastatic pancreatic cancer cell) or was not noticeably changed in PANC-1 at between 0.05–0.2 μM of CPPB. These biochemical data may support that a selective DPAGT1 inhibitor, CPPB is effective in inhibiting metastasis spread of the pancreatic cancer cells observed in scratch and transwell assays (Figures 5 and 6). Other than pancreatic cancers, a lower DPAGT1 expression cell, a colorectal adenocarcinoma (HCT-116) and a higher DPAGT1 expression cell, a cervical carcinoma (SiHa) were examined. CPPB did not inhibit migration of HCT-116, but strongly inhibited migration of SiHa in scratch assays at 0.2 μM (IC_{50} concentration against DPAGT1). These observations were supported by the

biochemical analyses of the Snail and E-cadherin expression levels. Snail plays an important role in cancer progression. The accumulated evidences on Snail indicate that over-expression of Snail promotes drug resistance, tumor recurrence and metastasis.[40] Although, only limited data have been generated in this article, CPPB's Snail inhibitory activity observed in pancreatic and a several high DPAGT1-expressed cell lines suggests that selective DPAGT1 inhibitors have the potential to develop into less toxic anticancer therapeutics than anticancer drugs that are cytotoxic to all dividing cells in the body. CPPB is not cytotoxic against a series of cancer and healthy cell lines at 10 μM or higher concentrations. However, it showed a cytostatic activity against pancreatic cancers and a strong synergistic effect with paclitaxel; cytotoxic activity of paclitaxel was improved over 250-times against PD002 in combination with CPPB (0.2–2.0 μM). Docking studies of CPPB with the available DPAGT1 crystal structures provided insight into unique interactions, and thus, structure-based molecule design may be a fruitful approach to improve CPPB's DPAGT1 affinity. A collaboration with Daiichi-Sankyo is essential to efficiently produce CPPB for *in vivo* studies using large-animal models such as dogs, pigs, and monkeys. We have demonstrated a semi-synthesis of CPPB from a capuramycin biosynthetic intermediate, A-500359F, that will secure a production of large amount of CPPB (Scheme 4). Our total synthetic scheme is amenable to produce gram-quantity of CPPB (Scheme 3). Extensive synergistic, toxicity, and pharmacokinetic studies of CPPB will be performed using preclinical animal models, and these data including detailed evaluation on *in vivo* efficacy against pancreatic and cervical cancers will be reported elsewhere.

EXPERIMENTAL SECTION

Chemistry. General Information.

All chemicals were purchased from commercial sources and used without further purification unless otherwise noted. THF, CH_2Cl_2, and DMF were purified via Innovative Technology's Pure-Solve System. All reactions were performed under an Argon atmosphere. All stirring was performed with an internal magnetic stirrer. Reactions were monitored by TLC using 0.25 mm coated commercial silica gel plates (EMD, Silica Gel $60F_{254}$). TLC spots were visualized by UV light at 254 nm, or developed with ceric ammonium molybdate or anisaldehyde or copper sulfate or ninhydrin solutions by heating on a hot plate. Reactions were also monitored by using SHIMADZU LCMS-2020 with solvents: A: 0.1% formic acid in water, B: acetonitrile. Flash chromatography was performed with SiliCycle silica gel (Purasil 60 Å, 230–400 Mesh). Proton magnetic resonance (^{1}H-NMR) spectral data were recorded on 400, and 500 MHz instruments. Carbon magnetic resonance (^{13}C-NMR) spectral data were recorded on 100 and 125 MHz instruments. For all NMR spectra, chemical shifts (δH, δC) were quoted in parts per million (ppm), and *J* values were quoted in Hz. ^{1}H and ^{13}C NMR spectra were calibrated with residual undeuterated solvent ($CDCl_3$: δH = 7.26 ppm, δC = 77.16 ppm; CD_3CN: δH = 1.94 ppm, δC = 1.32ppm; CD_3OD: δH =3.31 ppm, δC =49.00 ppm; DMSO-d_6: δH = 2.50 ppm, δC = 39.52 ppm; D_2O: δH = 4.79 ppm) as an internal reference. The following abbreviations were used to designate the multiplicities: s = singlet, d = doublet, dd = double doublets, t = triplet, q = quartet, quin = quintet, hept = heptet, m = multiplet, br = broad. Infrared (IR) spectra were recorded on a Perkin-Elmer FT1600 spectrometer. HPLC analyses were performed with a Shimadzu

LC-20AD HPLC system. HR-MS data were obtained from a Waters Synapt G2-Si (ion mobility mass spectrometer with nanoelectrospray ionization). All assayed compounds were purified by reverse HPLC to be ≥95% purity.

(2*S*,3*S*,4*S*,5*R*,6*R*)-2-((1*S*)-((2*R*,5*R*)-3-Acetoxy-5-(3-((benzyloxy)methyl)-2,4-dioxo-3,4-dihydropyrimidin-1(2*H*)-yl)-4-methoxytetrahydrofuran-2-yl)(cyano)methoxy)-6-((2-chloroacetoxy)methyl)tetrahydro-2*H*-pyran-3,4,5-triyl triacetate (15).

To a stirred suspension of **13** (0.17 g, 0.38 mmol), **14** (0.37 g, 0.75 mmol), MS3Å (0.50 g) and $SrCO_3$ (0.28 g, 1.88 mmol) in CH_2Cl_2 (9.4 mL) were added $AgBF_4$ (0.037 g, 0.19 mmol) and NIS (0.25 g, 1.13 mmol) at 0 °C. After being stirred for 19h, the reaction mixture was added Et_3N (1.0 mL) and passed through a silica gel pad (hexanes/EtOAc = 1/4). The filtrate was concentrated *in vacuo*. The crude mixture was purified by silica gel column chromatography (hexanes/EtOAc = 2/1 to 1/2) to afford **15** (0.24 g, 78%): ^{1}H NMR (400 MHz, Chloroform-*d*) δ 7.40 – 7.27 (m, 6H), 6.07 (d, *J* = 4.7 Hz, 1H), 6.00 (d, *J* = 8.2 Hz, 1H), 5.51 (d, *J* = 9.8 Hz, 1H), 5.47 (d, *J* = 9.6 Hz, 1H), 5.37 (dd, *J* = 3.4, 2.0 Hz, 1H), 5.28 (d, *J* = 10.2 Hz, 1H), 5.22 – 5.15 (m, 2H), 4.84 (d, *J* = 3.2 Hz, 1H), 4.71 (s, 2H), 4.41 (dd, *J* = 5.5, 3.2 Hz, 1H), 4.39 – 4.35 (m, 1H), 4.33 (d, *J* = 6.0 Hz, 1H), 4.27 (d, *J* = 2.3 Hz, 1H), 4.14 (d, *J* = 1.7 Hz, 2H), 4.03 – 4.01 (m, 1H), 3.93 (ddd, *J* = 8.9, 5.9, 2.4 Hz, 1H), 3.47 (s, 3H), 2.20 (s, 3H), 2.19 (s, 3H), 2.07 (s, 3H), 2.02 (s, 3H); ^{13}C NMR (101 MHz, $CDCl_3$) δ 170.20, 169.84, 169.50, 166.92, 162.19, 150.97, 137.75, 137.46, 128.32 (2C), 127.72, 127.69 (2C), 113.96, 103.58, 96.29, 88.68, 80.93, 80.09, 72.30, 70.42, 69.60, 68.46, 67.94, 65.16, 64.35, 63.58, 59.26, 40.61, 31.58, 20.70, 20.66, 20.62, 20.57; HRMS (ESI+) *m*/*z* calcd for $C_{35}H_{41}ClN_3O_{17}$ [M + H] 810.2125, found: 810.2151.

(2*R*,3*S*,4*S*,5*R*,6*R*)-2-((1*R*)-1-((2*S*,5*R*)-3-Acetoxy-5-(2,4-dioxo-3,4-dihydropyrimidin-1(2*H*)-yl)-4-methoxytetrahydrofuran-2-yl)-2-amino-2-oxoethoxy)-6-(hydroxymethyl)tetrahydro-2*H*-pyran-3,4,5-triyl triacetate (16).

To a stirred solution of **15** (0.24 g, 0.29 mmol) in a 9:1 mixture of EtOH and H_2O (2.9 mL) were added $HgCl_2$ (0.16 g, 0.59 mmol) and acetaldoxime (0.18 mL, 2.9 mmol). After being stirred for 13h at r.t., the reaction mixture was concentrated *in vacuo*. The residue was quenched with aq. $NaHCO_3$, and extracted with $CHCl_3$. The combined organic extracts were dried over Na_2SO_4 and concentrated *in vacuo*. The crude product was purified by silica gel column chromatography (hexanes/EtOAc = 1/2 to $CHCl_3$/MeOH = 96/4) to afford the amide (0.21 g, 87%). To a solution of the amide (0.21 g, 0.26 mmol) in a 1:1 mixture of THF and MeOH (2.6 mL) was added thiourea (0.059 g, 0.77 mmol). After being stirred for 11h at 50 °C, the reaction mixture was concentrated *in vacuo*. The residue was diluted with H_2O and extracted with $CHCl_3$. The combined organic extracts were dried over Na_2SO_4 and concentrated *in vacuo*. The crude product was purified by silica gel column chromatography ($CHCl_3$/MeOH = 98/2 to 97/3 to 96/4) to afford the primary alcohol (0.15 g, 75%). To a stirred solution of the primary alcohol (0.15 g, 0.19 mmol) and AcOH (0.040 mL) in a 1:1 mixture of THF and ^{i}PrOH (2.0 mL) was added 10% Pd/C (0.12 g) under N_2. H_2 gas was introduced and the reaction mixture was stirred under H_2 atmosphere for 3h, the solution was filtered through Celite and concentrated *in vacuo*. The crude product was purified by silica gel column chromatography ($CHCl_3$/MeOH = 97/3 to 92/8) to afford **16** (0.10 g, 81%): ^{1}H NMR (400 MHz, Chloroform-*d*) δ 9.08 (brs, 1H), 7.60 (d, *J* = 8.2 Hz, 1H), 6.87

(brs, 1H), 6.12 (brs, 1H), 6.00 (d, *J* = 8.1 Hz, 1H), 5.87 (d, *J* = 3.6 Hz, 1H), 5.55 – 5.52 (m, 1H), 5.26 – 5.22 (m, 2H), 5.20 (t, *J* = 6.0 Hz, 1H), 5.00 (d, *J* = 1.7 Hz, 1H), 4.53 (dd, *J* = 6.5, 2.3 Hz, 1H), 4.46 (d, *J* = 2.3 Hz, 1H), 4.06 (dd, *J* = 5.5, 3.7 Hz, 1H), 3.76 – 3.71 (m, 1H), 3.69 – 3.57 (m, 2H), 3.44 (s, 3H), 2.17 (s, 3H), 2.15 (s, 3H), 2.09 (s, 3H), 2.04 (s, 3H); ^{13}C NMR (101 MHz, $CDCl_3$) δ 171.42, 170.46, 170.46, 170.40, 163.10, 150.03, 139.50, 103.61, 97.15, 96.95, 88.50, 81.26, 80.96, 75.33, 72.91, 69.67, 68.89, 65.54, 61.27, 59.05, 50.86, 20.82, 20.75, 20.67, 20.59; HRMS (ESI+) *m*/*z* calcd for $C_{25}H_{34}N_3O_{16}$ [M + H] 632.1939, found: 632.1963.

(2*S*,3*S*,4*S*)-3,4-Diacetoxy-2-((1*R*)-1-((2*S*,5*R*)-3-acetoxy-5-(2,4-dioxo-3,4-dihydropyrimidin-1(2*H*)-yl)-4-methoxytetrahydrofuran-2-yl)-2-amino-2-oxoethoxy)-3,4-dihydro-2*H*-pyran-6-carboxylic acid (18).

To a stirred solution of **16** (0.10 g, 0.16 mmol) and DMSO (0.11 mL, 1.57 mmol) in a 5:1 mixture of CH_2Cl_2 and Et_3N (0.80 mL) was added SO_3•pyridine (0.25 g, 1.57 mmol). After being stirred for 3h at r.t., the reaction mixture was added H_2O (0.16 mL) and passed through a silica gel pad ($CHCl_3$/MeOH = 92/8) to provide the crude **17**. To a stirred solution of the crude mixture in ^{t}BuOH (1.0 mL) and 2-methyl-2-butene (0.5 mL) was added a solution of $NaClO_2$ (0.071 g, 0.78 mmol) and NaH_2PO_4•$2H_2O$ (0.12 g, 0.78 mmol) in H_2O (1.0 mL). After being stirred for 4h at r.t., the reaction was quenched with H_2O and extracted with $CHCl_3$/MeOH (9/1). The combined organic extracts were dried over Na_2SO_4 and concentrated *in vacuo*. The crude product was purified by silica gel column chromatography ($CHCl_3$/MeOH = 9/1) to afford **18** (0.078 g, 85%): ^{1}H NMR (400 MHz, Methanol-d_4) δ 7.77 (d, *J* = 8.1 Hz, 1H), 5.94 (d, *J* = 11.7 Hz, 1H), 5.94 (s, 1H), 5.78 (t, *J* = 2.1 Hz, 1H), 5.66 (dd, *J* = 4.5, 2.5 Hz, 1H), 5.56 (ddd, *J* = 4.7, 3.2, 1.6 Hz, 1H), 5.32 (d, *J* = 3.3 Hz, 1H), 4.99 (t, *J* = 5.2 Hz, 1H), 4.85 (d, *J* = 2.1 Hz, 1H), 4.60 (dd, *J* = 5.2, 2.0 Hz, 1H), 3.95 (t, *J* = 5.0 Hz, 1H), 3.39 (s, 3H), 2.13 (s, 3H), 2.08 (s, 3H), 2.05 (s, 3H); ^{13}C NMR (101 MHz, MeOD) δ 172.79, 172.06, 171.60, 167.79, 166.01, 152.05, 148.16, 140.97, 104.23, 103.98, 97.91, 88.13, 83.38, 82.91, 76.56, 71.95, 65.17, 65.06, 59.41, 20.75, 20.63, 20.57; HRMS (ESI+) *m*/*z* calcd for $C_{23}H_{28}N_3O_{15}$ [M + H] 586.1520, found: 586.1549.

(2*S*,3*S*,4*S*)-2-((1*R*)-1-((2*S*,5*R*)-3-Acetoxy-5-(2,4-dioxo-3,4-dihydropyrimidin-1(2*H*)-yl)-4-methoxytetrahydrofuran-2-yl)-2-amino-2-oxoethoxy)-6-(((S)-2-oxoazepan-3-yl)carbamoyl)-3,4-dihydro-2*H*-pyran-3,4-diyl diacetate (19).

To a stirred solution of **18** (31 mg, 0.053 mmol), 2-(*S*)-aminocaprolactam (26 mg, 0.16 mmol), HOBt (21 mg, 0.16 mmol) and NMM (58 μL, 0.53 mmol) in DMF (0.26 mL) was added EDCI (51 mg, 0.26 mmol). After being stirred for 6h at r.t., the reaction was quenched with aq. $NaHCO_3$, and extracted with $CHCl_3$/MeOH (9/1). The combined organic extracts were dried over Na_2SO_4 and concentrated *in vacuo*. The crude product was purified by silica gel column chromatography ($CHCl_3$/MeOH = 95/5) to afford **19** (30 mg, 82%): ^{1}H NMR (400 MHz, Methanol-d_4) δ 7.68 (d, *J* = 8.2 Hz, 1H), 6.02 (t, *J* = 2.1 Hz, 1H), 5.91 (d, *J* = 4.2 Hz, 1H), 5.89 (d, *J* = 6.3 Hz, 1H), 5.73 (dd, *J* = 4.4, 2.5 Hz, 1H), 5.68 – 5.65 (m, 1H), 5.51 (d, *J* = 3.0 Hz, 1H), 5.01 (d, *J* = 4.6 Hz, 1H), 4.76 (d, *J* = 2.0 Hz, 1H), 4.62 (d, *J* = 12.5 Hz, 1H), 4.60 – 4.57 (m, 1H), 3.98 (d, *J* = 6.1 Hz, 1H), 3.35 (s, 3H), 2.11 (s, 3H), 2.08 (s, 3H), 2.05 (s, 3H), 2.03 – 1.98 (m, 2H), 1.91 – 1.83 (m, 2H), 1.65 – 1.56 (m, 2H), 1.44 – 1.37 (m, 2H); ^{13}C NMR (101 MHz, MeOD) δ 176.12, 172.32, 171.66, 171.29, 171.21, 165.96,

160.96, 151.90, 144.61, 141.42, 106.25, 103.54, 98.81, 88.77, 83.41, 79.28, 77.39, 74.79, 64.91, 64.49, 59.26, 57.36, 53.25, 42.36, 32.19, 29.75, 28.94, 20.54, 20.41, 20.32; HRMS (ESI+) *m*/*z* calcd for $C_{29}H_{38}N_5O_{15}$ [M + H] 696.2364, found: 696.2391.

(2*S*,3*S*,4*S*)-2-((1*R*)-2-Amino-1-((2*S*,5*R*)-5-(2,4-dioxo-3,4-dihydropyrimidin-1(2*H*)-yl)-3-hydroxy-4-methoxytetrahydrofuran-2-yl)-2-oxoethoxy)-3,4-dihydroxy-*N*-((*S*)-2-oxoazepan-3-yl)-3,4-dihydro-2*H*-pyran-6-carboxamide (3).

A solution of **19** (30 mg, 0.043 mmol) in a 5:1 mixture of MeOH and Et_3N (0.60 mL) was stirred for 5h at r.t., and concentrated *in vacuo*. The crude mixture was purified by reverse-phase HPLC [column: Luna® (C18, 10 μm, 100 Å, 250 × 10 mm), solvents: 15:85 MeOH:H_2O, flow rate: 3.0 mL/min, UV: 254 nm, retention time: 20 min] to afford I-CAP (**3**, 24 mg, 98%): ^{1}H NMR (400 MHz, Methanol-d_4) δ 7.92 (d, *J* = 8.1 Hz, 1H), 6.02 (d, *J* = 3.8 Hz, 1H), 5.88 (d, *J* = 5.1 Hz, 1H), 5.74 (d, *J* = 8.1 Hz, 1H), 5.23 (d, *J* = 5.6 Hz, 1H), 4.67 (d, *J* = 2.0 Hz, 1H), 4.59 – 4.54 (m, 2H), 4.38 (t, *J* = 4.2 Hz, 1H), 4.29 (t, *J* = 5.1 Hz, 1H), 3.98 (t, *J* = 5.0 Hz, 1H), 3.84 (t, *J* = 4.6 Hz, 1H), 3.43 (s, 3H), 2.06 – 1.99 (m, 2H), 1.89 – 1.81 (m, 2H), 1.62 – 1.45 (m, 2H), 1.44 – 1.33 (m, 2H); ^{13}C NMR (101 MHz, MeOD) δ 176.27, 173.46, 166.15, 161.85, 152.32, 144.23, 141.91, 109.37, 102.82, 101.22, 90.27, 83.49, 81.02, 78.93, 74.54, 68.51, 63.53, 58.67, 53.35, 42.48, 32.36, 29.91, 29.06; HRMS (ESI+) *m*/*z* calcd for $C_{23}H_{32}N_5O_{12}$ [M + H] 570.2048, found: 570.2071.

(2*S*,3*S*,4*S*,5*R*,6*R*)-2-((*S*)-((3a*R*,4*R*,6R,6a*R*)-6-(3-((Benzyloxy)methyl)-2,4-dioxo-3,4-dihydropyrimidin-1(2*H*)-yl)-2,2-dimethyltetrahydrofuro[3,4-*d*][1,3]dioxol-4-yl)(cyano)methoxy)-6-((2-chloroacetoxy)methyl)tetrahydro-2*H*-pyran-3,4,5-triyl triacetate (21).

To a stirred suspension of **20** (0.24 g, 0.56 mmol), **14** (0.55 g, 1.12 mmol), MS3Å (0.72 g), and $SrCO_3$ (0.41 g, 2.80 mmol) in CH_2Cl_2 (14.0 mL) were added $AgBF_4$ (0.055 g, 0.28 mmol) and NIS (0.25 g, 1.12 mmol) at 0 °C. After being stirred for 12h, the reaction mixture was added Et_3N (1.0 mL), and passed through a silica gel pad (hexanes/EtOAc = 1/4). The filtrate was concentrated *in vacuo*. The crude mixture was purified by silica gel column chromatography (hexanes/EtOAc = 6/4 – 4/6) to afford **21** (0.39 g, 88%): ^{1}H NMR (400 MHz, Chloroform-*d*) δ 7.37 – 7.28 (m, 5H), 7.20 (d, *J* = 8.1 Hz, 1H), 5.82 (d, *J* = 8.1 Hz, 1H), 5.61 (d, *J* = 1.6 Hz, 1H), 5.50 (d, *J* = 9.8 Hz, 1H), 5.42 (d, *J* = 9.8 Hz, 1H), 5.35 – 5.27 (m, 1H), 5.23 (dd, *J* = 10.0, 3.3 Hz, 1H), 5.07 (d, *J* = 1.9 Hz, 1H), 5.00 (d, *J* = 3.5 Hz, 1H), 4.98 (dd, *J* = 6.4, 1.6 Hz, 1H), 4.84 (d, *J* = 7.1 Hz, 1H), 4.69 (s, 2H), 4.43 (dd, *J* = 7.1, 3.6 Hz, 1H), 4.20 (dd, *J* = 12.2, 4.3 Hz, 1H), 4.17 – 4.07 (m, 2H), 4.05 (d, *J* = 1.6 Hz, 2H), 3.97 – 3.92 (m, 1H), 2.16 (s, 3H), 2.02 (s, 3H), 1.98 (s, 3H), 1.59 (s, 3H), 1.39 (s, 3H); ^{13}C NMR (101 MHz, $CDCl_3$) δ 169.80, 169.57, 169.47, 166.80, 162.08, 150.84, 140.89, 137.67, 128.33 (2C), 127.91, 127.77, 127.63 (2C), 115.23, 114.72, 102.84, 96.56, 96.30, 86.55, 84.15, 80.95, 72.42, 70.41, 69.41, 68.39 (2C), 66.04, 65.35, 62.90, 40.52, 27.03, 25.20, 20.73, 20.64, 20.59; HRMS (ESI+) *m*/*z* calcd for $C_{35}H_{41}ClN_3O_{16}$ [M + H] 794.2175, found: 794.2198.

(2*R*,3*S*,4*S*,5*R*,6*R*)-2-((*R*)-2-Amino-1-((3a*R*,4*S*,6*R*,6a*R*)-6-(2,4-dioxo-3,4-dihydropyrimidin-1(2*H*)-yl)-2,2-dimethyltetrahydrofuro[3,4-*d*][1,3]dioxol-4-yl)-2-oxoethoxy)-6-(hydroxymethyl)tetrahydro-2*H*-pyran-3,4,5-triyl triacetate (22).

To a stirred solution of **21** (0.39 g, 0.49 mmol) in a 9:1 mixture of EtOH and H_2O (4.9 mL) were added $HgCl_2$ (0.27 g, 0.98 mmol) and acetaldoxime (0.30 mL, 4.9 mmol). After being stirred for 12h at r.t., the reaction mixture was concentrated *in vacuo*. The residue was diluted with aq.$NaHCO_3$, and extracted with $CHCl_3$. The combined organic extracts were dried over Na_2SO_4 and concentrated *in vacuo*. The crude product was purified by silica gel column chromatography (hexanes/EtOAc = 1/2 to $CHCl_3$/MeOH = 97/3) to afford the amide (0.36 g, 91%). To a solution of the amide (0.36 g, 0.45 mmol) in a 1:1 mixture of THF and MeOH (4.5 mL) was added thiourea (0.10 g, 1.34 mmol). After being stirred for 11h at 50 °C, the reaction mixture was concentrated *in vacuo*. The residue was diluted with H_2O, and extracted with $CHCl_3$. The combined organic extracts were dried over Na_2SO_4 and concentrated *in vacuo*. The crude product was purified by silica gel column chromatography ($CHCl_3$/MeOH = 98/2 to 97/3 to 96/4) to afford the primary alcohol (0.25 g, 76%). To a stirred solution of the alcohol (0.25 g, 0.34 mmol) and AcOH (0.08 mL) in a 1:1 mixture of THF and ^{i}PrOH (4.0 mL) was added 10% Pd/C (0.20 g) under N_2. H_2 gas was introduced and the reaction mixture was stirred under H_2 atmosphere. After being stirred for 4h at r.t., the reaction mixture was filtered through Celite and concentrated *in vacuo*. The crude product was purified by silica gel column chromatography ($CHCl_3$/MeOH = 96/4 to 92/8) to afford **22** (0.17 g, 80%): ^{1}H NMR (400 MHz, Chloroform-*d*) δ 9.45 (brs, 1H), 7.34 (d, *J* = 8.0 Hz, 1H), 6.72 (brs, 1H), 6.17 (brs, 1H), 5.78 (d, *J* = 8.0 Hz, 1H), 5.60 (d, *J* = 1.7 Hz, 1H), 5.43 (dd, *J* = 10.1, 3.5 Hz, 1H), 5.33 (dd, *J* = 3.5, 1.7 Hz, 1H), 5.20 (t, *J* = 10.1 Hz, 1H), 5.12 – 5.05 (m, 1H), 5.03 (dd, *J* = 6.4, 1.7 Hz, 1H), 4.98 (s, 1H), 4.46 (d, *J* = 5.8 Hz, 1H), 4.33 (t, *J* = 5.1 Hz, 1H), 3.88 (dt, *J* = 10.1, 4.0 Hz, 1H), 3.60 – 3.53 (m, 2H), 2.14 (s, 3H), 2.07 (s, 3H), 2.02 (s, 3H), 1.55 (s, 3H), 1.35 (s, 3H); ^{13}C NMR (101 MHz, $CDCl_3$) δ 170.68, 170.40, 170.28, 170.24, 163.27, 150.13, 142.81, 114.72, 102.85, 96.39, 87.34, 84.26, 80.35, 71.92, 69.35, 68.64, 66.03, 61.16, 27.25, 25.42, 20.83, 20.77, 20.74; HRMS (ESI+) *m*/*z* calcd for $C_{25}H_{34}N_3O_{15}$ [M + H] 616.1990, found: 616.2018.

(2*S*,3*S*,4*S*)-2-((*R*)-2-Amino-1-((3a*R*,4*S*,6*R*,6a*R*)-6-(2,4-dioxo-3,4-dihydropyrimidin-1(2*H*)-yl)-2,2-dimethyltetrahydrofuro[3,4-*d*][1,3]dioxol-4-yl)-2-oxoethoxy)-6-(((*S*)-2-oxoazepan-3-yl)carbamoyl)-3,4-dihydro-2*H*-pyran-3,4-diyl diacetate (23).

To a stirred solution of **22** (0.17 g, 0.27 mmol) and DMSO (0.19 mL, 2.72 mmol) in a 5:1 mixture of CH_2Cl_2 and Et_3N (1.4 mL) was added SO_3•pyridine (0.43 g, 2.72 mmol). After being stirred for 3h at r.t., the reaction mixture was added H_2O (0.27 mL) and passed through a silica gel pad ($CHCl_3$/MeOH = 92/8). To a stirred solution of the crude mixture in ^{t}BuOH (1.0 mL) and 2-methyl-2-butene (0.5 mL) was added a solution of $NaClO_2$ (0.12 g, 1.36 mmol) and NaH_2PO_4•$2H_2O$ (0.21 g, 1.36 mmol) in H_2O (1.0 mL). After being stirred for 5h at r.t., the reaction was extracted with $CHCl_3$/MeOH (9/1). The combined organic extracts were dried over Na_2SO_4 and concentrated *in vacuo*. The crude product was purified by silica gel column chromatography ($CHCl_3$/MeOH = 9/1) to afford the acid (0.13 g, 81%). To a stirred solution of the acid (28 mg, 0.049 mmol), 2-(*S*)-aminocaprolactam (24 mg, 0.15 mmol), HOBt (20 mg, 0.15 mmol) and NMM (54 μL, 0.49 mmol) in DMF (0.25 mL) was

added EDCI (47 mg, 0.25 mmol). After being stirred for 14h at r.t., the reaction was quenched with aq.$NaHCO_3$, and extracted with $CHCl_3$/MeOH (9/1). The combined organic extracts were dried over Na_2SO_4 and concentrated *in vacuo*. The crude product was purified by silica gel column chromatography ($CHCl_3$/MeOH = 95/5) to afford **23** (30 mg, 89%): ^{1}H NMR (400 MHz, Methanol-d_4) δ 7.79 (d, *J* = 8.0 Hz, 1H), 5.98 (t, *J* = 2.0 Hz, 1H), 5.84 (d, *J* = 2.8 Hz, 1H), 5.78 (d, *J* = 8.0 Hz, 1H), 5.62 (dd, *J* = 4.5, 2.6 Hz, 1H), 5.51 – 5.48 (m, 1H), 5.45 (d, *J* = 3.1 Hz, 1H), 4.74 (d, *J* = 2.8 Hz, 1H), 4.71 (dd, *J* = 6.2, 2.9 Hz, 1H), 4.65 (dd, *J* = 6.2, 3.3 Hz, 1H), 4.59 – 4.55 (m, 2H), 3.76 – 3.67 (m, 4H), 2.09 (s, 3H), 2.04 (s, 3H), 1.86 (d, *J* = 13.4 Hz, 3H), 1.63 – 1.52 (m, 3H), 1.51 (s, 3H), 1.45 – 1.34 (m, 3H), 1.25 (s, 3H); ^{13}C NMR (101 MHz, MeOD) δ 176.35, 172.24, 171.62, 171.28, 166.24, 161.14, 151.99, 144.75, 142.76, 115.34, 106.38, 102.91, 98.75, 93.55, 87.12, 85.94, 82.02, 78.13, 67.16, 64.99, 64.46, 56.04, 53.46, 46.10, 42.52, 42.43, 32.25, 29.89, 29.08, 27.47, 25.47, 20.61, 20.52; HRMS (ESI+) *m*/*z* calcd for $C_{29}H_{38}N_5O_{14}$ [M + H] 680.2415, found: 680.2432.

(2*S*,3*S*,4*S*)-2-((1*R*)-2-Amino-1-((2*S*,5*R*)-5-(2,4-dioxo-3,4-dihydropyrimidin-1(2*H*)-yl)-3,4-dihydroxytetrahydrofuran-2-yl)-2-oxoethoxy)-3,4-dihydroxy-*N*-((*S*)-2-oxoazepan-3-yl)-3,4-dihydro-2*H*-pyran-6-carboxamide (4).

A solution of **23** (30 mg, 0.044 mmol) in a 4:1 mixture of TFA and H_2O (0.88 mL) was stirred for 4h at r.t., and concentrated *in vacuo*. A solution of the crude diol in a 5:1 mixture of MeOH and Et_3N (0.88 mL) was stirred for 9h at r.t., filtered, and concentrated *in vacuo*. The crude mixture was purified by reverse-phase HPLC [column: Luna® (C18, 10 μm, 100 Å, 250 × 10 mm), solvents: 15:85 MeOH:H_2O, flow rate: 3.0 mL/min, UV: 254 nm, retention time: 16 min] to afford DM-CAP (**4**, 22 mg, 90%): ^{1}H NMR (400 MHz, Methanol-d_4) δ 7.94 (d, *J* = 8.1 Hz, 1H), 6.03 (d, *J* = 4.5 Hz, 1H), 5.85 (d, *J* = 3.7 Hz, 1H), 5.73 (d, *J* = 8.2 Hz, 1H), 5.19 (d, *J* = 6.7 Hz, 1H), 4.68 (d, *J* = 1.7 Hz, 1H), 4.61 (dd, *J* = 11.2, 1.4 Hz, 1H), 4.54 (dd, *J* = 5.8, 1.7 Hz, 1H), 4.36 (t, *J* = 4.5 Hz, 1H), 4.30 (t, *J* = 5.5 Hz, 1H), 4.12 (t, *J* = 4.4 Hz, 1H), 3.97 (t, *J* = 5.7 Hz, 1H), 3.90 (t, *J* = 6.5 Hz, 1H), 3.43 – 3.38 (m, 1H), 3.03 (t, *J* = 7.0 Hz, 1H), 2.70 – 2.64 (m, 1H), 2.07 – 1.97 (m, 2H), 1.81 (d, *J* = 15.2 Hz, 2H), 1.62 (q, *J* = 11.9, 10.7 Hz, 1H), 1.39 (s, 1H); ^{13}C NMR (101 MHz, MeOD) δ 176.85, 174.05, 166.21, 162.02, 152.21, 144.60, 141.91, 108.72, 102.50, 101.60, 90.76, 84.77, 79.50, 75.68, 71.40, 63.63, 60.06, 53.44, 42.50, 31.89, 29.82, 29.14; HRMS (ESI+) *m*/*z* calcd for $C_{22}H_{30}N_5O_{12}$ [M + H] 556.1891, found: 556.1912.

(2*S*,3*S*,4*S*)-2-((1*R*)-1-((2*S*,5*R*)-4-Acetoxy-5-(2,4-dioxo-3,4-dihydropyrimidin-1(2*H*)-yl)-3-methoxytetrahydrofuran-2-yl)-2-amino-2-oxoethoxy)-6-((4-(4-(4-(trifluoromethoxy)phenoxy)piperidin-1-yl)benzyl)carbamoyl)-3,4-dihydro-2*H*-pyran-3,4-diyl diacetate (37).

To a stirred solution of **32** (55 mg, 0.094 mmol), **34** (0.10 g, 0.28 mmol), HOBt (38 mg, 0.28 mmol) and NMM (95 μL, 0.94 mmol) in DMF (0.47 mL) was added EDCI (90 mg, 0.47 mmol). After being stirred for 7h at r.t., the reaction mixture was quenched with aq.$NaHCO_3$, and extracted with $CHCl_3$/MeOH (9/1). The combined organic extracts were dried over Na_2SO_4 and concentrated *in vacuo*. The crude product was purified by silica gel column chromatography ($CHCl_3$/MeOH = 95/5) to afford **37** (76 mg, 87%): ^{1}H NMR (400 MHz, Methanol-d_4) δ 7.71 (d, *J* = 8.1 Hz, 1H), 7.23 (d, *J* = 8.5 Hz, 2H), 7.19 (d, *J* = 8.8 Hz, 2H), 7.03 (d, *J* = 9.1 Hz, 2H), 6.97 (d, *J* = 8.7 Hz, 2H), 5.97 (t, *J* = 2.1 Hz, 1H), 5.91 (d, *J* =

8.1 Hz, 1H), 5.87 (d, *J* = 3.8 Hz, 1H), 5.74 (dd, *J* = 4.5, 2.4 Hz, 1H), 5.67 (ddd, *J* = 4.5, 2.8, 1.7 Hz, 1H), 5.43 (d, *J* = 2.8 Hz, 1H), 5.28 (dd, *J* = 5.1, 3.8 Hz, 1H), 4.70 (d, *J* = 1.9 Hz, 1H), 4.54 (dq, *J* = 7.5, 3.8 Hz, 1H), 4.42 (d, *J* = 14.5 Hz, 1H), 4.38 (dd, *J* = 6.2, 1.9 Hz, 1H), 4.33 (d, *J* = 14.4 Hz, 1H), 3.82 – 3.79 (m, 1H), 3.48 (td, *J* = 9.0, 6.8, 3.5 Hz, 3H), 3.13 – 3.06 (m, 2H), 3.05 (s, 3H), 2.09 (s, 3H), 2.09 (s, 3H), 2.06 (s, 3H), 1.87 (dtd, *J* = 12.3, 8.2, 3.6 Hz, 3H); ^{13}C NMR (101 MHz, MeOD) δ 172.85, 171.84, 171.43, 171.17, 166.07, 162.39, 157.61, 152.11, 151.92, 144.94, 143.92, 141.57, 130.89, 130.02 (2C), 123.59 (2C), 118.04 (2C), 117.98 (2C), 106.19, 103.75, 98.26, 89.36, 83.17, 78.98, 76.60, 74.71, 73.98, 64.75, 59.35, 48.18, 48.16, 31.43 (2C), 20.70, 20.52, 20.49; HRMS (ESI+) *m*/*z* calcd for $C_{42}H_{47}F_3N_5O_{16}$ [M + H] 934.2970, found 934.2998.

(2*S*,3*S*,4*S*)-2-((1*R*)-2-Amino-1-((2*S*,5*R*)-5-(2,4-dioxo-3,4-dihydropyrimidin-1(2*H*)-yl)-4-hydroxy-3-methoxytetrahydrofuran-2-yl)-2-oxoethoxy)-3,4-dihydroxy-*N*-(4-(4-(4-(trifluoromethoxy)phenoxy)piperidin-1-yl)benzyl)-3,4-dihydro-2*H*-pyran-6-carboxamide (5).

A solution of **37** (76 mg, 0.082 mmol) in a 5:1 mixture of MeOH and Et_3N (1.6 mL) was stirred for 6h at r.t., and concentrated *in vacuo*. The crude mixture was purified by reverse-phase HPLC [column: Luna® (C18, 10 μm, 100 Å, 250 × 10 mm), solvents: 65:35 MeOH:H_2O, flow rate: 3.0 mL/min, UV: 254 nm, retention time: 18 min] to afford CPPB (**5**, 63 mg, 95%): ^{1}H NMR (400 MHz, Methanol-d_4) δ 7.86 (d, *J* = 8.1 Hz, 1H), 7.20 (dd, *J* = 10.9, 8.6 Hz, 4H), 7.02 (d, *J* = 9.1 Hz, 2H), 6.97 (d, *J* = 8.7 Hz, 2H), 5.98 (dd, *J* = 3.3, 1.0 Hz, 1H), 5.80 (d, *J* = 4.4 Hz, 1H), 5.76 (d, *J* = 8.2 Hz, 1H), 5.21 (d, *J* = 4.6 Hz, 1H), 4.68 (d, *J* = 2.0 Hz, 1H), 4.54 (dp, *J* = 7.3, 3.6 Hz, 1H), 4.48 (dd, *J* = 5.2, 2.0 Hz, 1H), 4.44 (d, *J* = 14.5 Hz, 1H), 4.39 (t, *J* = 3.9 Hz, 1H), 4.33 (d, *J* = 14.6 Hz, 1H), 4.20 (t, *J* = 4.7 Hz, 1H), 4.06 – 4.02 (m, 1H), 3.66 (t, *J* = 5.1 Hz, 1H), 3.52 – 3.45 (m, 3H), 3.19 (s, 3H), 3.08 (ddd, *J* = 12.3, 8.6, 3.4 Hz, 3H), 2.15 – 2.07 (m, 2H), 1.86 (dtd, *J* = 12.2, 8.3, 3.5 Hz, 3H); ^{13}C NMR (101 MHz, MeOD) δ 173.68, 166.16, 163.31, 157.62, 152.18, 152.08, 144.15, 141.83, 130.91, 129.76 (2C), 123.58 (2C), 118.03 (4C), 109.58, 102.74, 100.64, 90.83, 83.32, 80.35, 77.51, 74.27, 74.01, 67.61, 63.48, 58.61, 48.20 (2C), 43.51, 31.47 (2C); HRMS (ESI+) *m*/*z* calcd for $C_{36}H_{41}F_3N_5O_{13}$ [M + H] 808.2653, found 808.2675.

(2*S*,3*S*,4*S*)-2-((1*R*)-1-((2*S*,5*R*)-3-Acetoxy-5-(2,4-dioxo-3,4-dihydropyrimidin-1(2*H*)-yl)-4-methoxytetrahydrofuran-2-yl)-2-amino-2-oxoethoxy)-6-((4-(4-(4-(trifluoromethoxy)phenoxy)piperidin-1-yl)benzyl)carbamoyl)-3,4-dihydro-2*H*-pyran-3,4-diyl diacetate (35).

To a stirred solution of **18** (33 mg, 0.056 mmol), **34** (62 mg, 0.17 mmol), HOBt (23 mg, 0.17 mmol) and NMM (62 μL, 0.56 mmol) in DMF (0.28 mL) was added EDCI (54 mg, 0.28 mmol). After being stirred for 14h at r.t., the reaction was quenched with aq.$NaHCO_3$, and extracted with $CHCl_3$/MeOH (9/1). The combined organic extracts were dried over Na_2SO_4 and concentrated *in vacuo*. The crude product was purified by silica gel column chromatography ($CHCl_3$/MeOH = 95/5) to afford **35** (43 mg, 82%): ^{1}H NMR (400 MHz, Methanol-d_4) δ 7.69 (d, *J* = 8.2 Hz, 1H), 7.22 (d, *J* = 8.5 Hz, 2H), 7.19 (d, *J* = 8.6 Hz, 2H), 7.02 (d, *J* = 9.0 Hz, 2H), 6.98 (d, *J* = 8.4 Hz, 2H), 5.99 – 5.97 (m, 1H), 5.95 (d, *J* = 5.8 Hz, 1H), 5.91 (d, *J* = 8.1 Hz, 1H), 5.74 – 5.71 (m, 1H), 5.66 – 5.63 (m, 1H), 5.46 (d, *J* = 3.2 Hz, 1H), 5.05 (t, *J* = 4.7 Hz, 1H), 4.78 (d, *J* = 2.0 Hz, 1H), 4.57 – 4.52 (m, 1H), 4.49 (d, *J* = 14.5 Hz, 1H), 4.39 – 4.34 (m, 1H), 4.30 (d, *J* = 14.7 Hz, 1H), 3.84 – 3.80 (m, 1H), 3.64 (s, 3H),

3.53 – 3.45 (m, 2H), 3.13 – 3.06 (m, 2H), 2.83 (t, *J* = 6.5 Hz, 1H), 2.10 (s, 3H), 2.07 (s, 3H), 2.06 (s, 3H), 1.87 (dtd, *J* = 12.7, 8.5, 3.5 Hz, 3H); ^{13}C NMR (101 MHz, MeOD) δ 172.92, 171.74, 171.36, 170.39, 166.18, 162.23, 157.56, 152.06, 151.81, 145.05, 140.90, 130.78, 129.96 (2C), 123.52 (2C), 117.96 (2C), 117.92 (2C), 105.75, 103.47, 98.22, 88.92, 82.72, 78.21, 76.44, 73.95, 67.92, 64.42, 61.21, 58.65, 58.20, 48.10 (2C), 43.57, 31.38 (2C), 20.60, 20.44, 20.39; HRMS (ESI+) *m*/*z* calcd for $C_{42}H_{47}F_3N_5O_{16}$ [M + H] 934.2970, found 934.2991.

(2*S*,3*S*,4*S*)-2-((1*R*)-2-Amino-1-((2*S*,5*R*)-5-(2,4-dioxo-3,4-dihydropyrimidin-1(2*H*)-yl)-3-hydroxy-4-methoxytetrahydrofuran-2-yl)-2-oxoethoxy)-3,4-dihydroxy-*N*-(4-(4-(4-(trifluoromethoxy)phenoxy)piperidin-1-yl)benzyl)-3,4-dihydro-2*H*-pyran-6-carboxamide (6).

A solution of **35** (43 mg, 0.046 mmol) in a 5:1 mixture of MeOH and Et_3N (0.92 mL) was stirred for 6h at r.t., and concentrated *in vacuo*. The crude mixture was purified by reverse-phase HPLC [column: Luna® (C18, 10 μm, 100 Å, 250 × 10 mm), solvents: 65:35 MeOH:H_2O, flow rate: 3.0 mL/min, UV: 254 nm, retention time: 19 min] to afford I-CPPB (**6**, 35 mg, 93%): ^{1}H NMR (400 MHz, Methanol-d_4) δ 7.79 (d, *J* = 8.2 Hz, 1H), 7.19 (d, *J* = 8.6 Hz, 4H), 7.02 (d, *J* = 9.1 Hz, 2H), 6.98 (d, *J* = 8.5 Hz, 2H), 5.98 (d, *J* = 3.6 Hz, 1H), 5.94 (d, *J* = 5.1 Hz, 1H), 5.77 (d, *J* = 8.0 Hz, 1H), 5.36 (d, *J* = 5.8 Hz, 1H), 4.67 – 4.65 (m, 1H), 4.61 (d, *J* = 2.8 Hz, 1H), 4.48 (dd, *J* = 8.6, 4.6 Hz, 1H), 4.36 – 4.33 (m, 1H), 4.27 (dd, *J* = 5.4, 2.7 Hz, 1H), 3.71 – 3.65 (m, 2H), 3.51 (d, *J* = 4.4 Hz, 2H), 3.48 (s, 3H), 3.25 – 3.18 (m, 2H), 2.13 – 2.00 (m, 3H), 1.92 – 1.76 (m, 3H); ^{13}C NMR (101 MHz, MeOD) δ 173.68, 166.15, 163.30, 157.62, 152.18, 152.08, 144.15, 141.83, 130.90, 129.76 (2C), 123.58 (2C), 118.10 (2C), 118.02 (2C), 109.57, 102.73, 100.63, 90.83, 83.32, 80.35, 77.51, 74.27, 74.01, 67.61, 63.48, 58.61, 48.20 (2C), 43.51, 31.47 (2C); HRMS (ESI+) *m*/*z* calcd for $C_{36}H_{41}F_3N_5O_{13}$ [M + H] 808.2653, found 808.2668.

(2*S*,3*S*,4*S*)-2-((1*R*)-2-Amino-1-((2*S*,5*R*)-5-(2,4-dioxo-3,4-dihydropyrimidin-1(2*H*)-yl)-3,4-dimethoxytetrahydrofuran-2-yl)-2-oxoethoxy)-6-((4-(4-(4-(trifluoromethoxy)phenoxy)piperidin-1-yl)benzyl)carbamoyl)-3,4-dihydro-2*H*-pyran-3,4-diyl diacetate (38).

To a stirred solution of **33** (38 mg, 0.068 mmol), **34** (75 mg, 0.20 mmol), HOBt (28 mg, 0.20 mmol) and NMM (75 μL, 0.68 mmol) in DMF (0.34 mL) was added EDCI (65 mg, 0.34 mmol). After being stirred for 7h at r.t., the reaction was quenched with aq.$NaHCO_3$, and extracted with $CHCl_3$/MeOH (9/1). The combined organic extracts were dried over Na_2SO_4 and concentrated *in vacuo*. The crude product was purified by silica gel column chromatography ($CHCl_3$/MeOH = 95/5) to afford **38** (53 mg, 86%): ^{1}H NMR (400 MHz, Methanol-d_4) δ 7.75 (d, *J* = 8.2 Hz, 1H), 7.24 (d, *J* = 8.6 Hz, 2H), 7.19 (d, *J* = 8.8 Hz, 2H), 7.02 (d, *J* = 9.1 Hz, 2H), 6.98 (d, *J* = 8.5 Hz, 2H), 5.98 (d, *J* = 2.0 Hz, 1H), 5.96 (d, *J* = 8.1 Hz, 1H), 5.85 (d, *J* = 2.9 Hz, 1H), 5.71 – 5.66 (m, 2H), 5.43 (d, *J* = 2.3 Hz, 1H), 4.70 (d, *J* = 1.9 Hz, 1H), 4.57 – 4.51 (m, 1H), 4.45 – 4.40 (m, 2H), 4.34 (d, *J* = 14.4 Hz, 1H), 3.86 (dd, *J* = 4.9, 2.9 Hz, 1H), 3.79 (t, *J* = 6.5 Hz, 1H), 3.60 (dd, *J* = 6.9, 4.9 Hz, 1H), 3.50 (td, *J* = 7.6, 7.0, 3.3 Hz, 2H), 3.46 (s, 3H), 3.11 (dd, *J* = 8.9, 3.6 Hz, 1H), 3.08 (s, 3H), 2.83 (t, *J* = 6.5 Hz, 1H), 2.14 (dd, *J* = 8.7, 5.4 Hz, 1H), 2.10 (s, 3H), 2.07 (s, 3H), 1.87 (dtd, *J* = 12.5, 8.2, 3.5 Hz, 2H); ^{13}C NMR (101 MHz, MeOD) δ 172.98, 171.81, 171.42, 166.22, 162.30, 157.62, 152.12, 151.87, 145.11, 140.96, 130.85, 130.02 (2C), 123.58 (2C), 118.03 (2C),

117.98 (2C), 105.81, 103.54, 98.28, 88.98, 82.79, 82.54, 78.28, 76.50, 74.02, 64.59, 64.49, 61.28, 58.72, 58.27, 48.17 (2C), 43.64, 42.08, 31.45 (2C), 20.67, 20.51; HRMS (ESI+) *m*/*z* calcd for $C_{41}H_{47}F_3N_5O_{15}$ [M + H] 906.3021, found 906.3045.

(2*S*,3*S*,4*S*)-2-((1*R*)-2-Amino-1-((2*S*,5*R*)-5-(2,4-dioxo-3,4-dihydropyrimidin-1(2*H*)-yl)-3,4-dimethoxytetrahydrofuran-2-yl)-2-oxoethoxy)-3,4-dihydroxy-*N*-(4-(4-(4-(trifluoromethoxy)phenoxy)piperidin-1-yl)benzyl)-3,4-dihydro-2*H*-pyran-6-carboxamide (7).

A solution of **38** (53 mg, 0.059 mmol) in a 5:1 mixture of MeOH and Et_3N (1.2 mL) was stirred for 6h at r.t., and concentrated *in vacuo*. The crude mixture was purified by reverse-phase HPLC [column: Luna® (C18, 10 μm, 100 Å, 250 × 10 mm), solvents: 65:35 MeOH:H_2O, flow rate: 3.0 mL/min, UV: 254 nm, retention time: 21 min] to afford OM-CPPB (**7**, 46 mg, 96%): ^{1}H NMR (400 MHz, Methanol-d_4) δ 7.89 (d, *J* = 8.1 Hz, 1H), 7.22 (d, *J* = 8.4 Hz, 2H), 7.19 (d, *J* = 8.7 Hz, 2H), 7.02 (d, *J* = 9.1 Hz, 2H), 6.96 (d, *J* = 8.5 Hz, 2H), 5.98 (dd, *J* = 3.0, 1.2 Hz, 1H), 5.85 (d, *J* = 3.3 Hz, 1H), 5.76 (d, *J* = 8.1 Hz, 1H), 5.22 (d, *J* = 4.1 Hz, 1H), 4.67 (d, *J* = 1.9 Hz, 1H), 4.57 – 4.51 (m, 1H), 4.46 (dd, *J* = 6.8, 2.0 Hz, 1H), 4.43 (d, *J* = 14.9 Hz, 1H), 4.40 (d, *J* = 3.7 Hz, 1H), 4.32 (d, *J* = 14.5 Hz, 1H), 4.08 (t, *J* = 4.2 Hz, 1H), 3.90 (t, *J* = 4.1 Hz, 1H), 3.70 (t, *J* = 5.5 Hz, 1H), 3.52 – 3.47 (m, 2H), 3.45 (s, 3H), 3.13 (s, 3H), 3.08 (td, *J* = 9.1, 4.6 Hz, 2H), 2.15 – 2.09 (m, 2H), 1.91 – 1.82 (m, 2H); ^{13}C NMR (101 MHz, MeOD) δ 173.61, 166.17, 163.21, 157.62, 152.09, 151.92, 144.02, 141.57, 130.94, 129.89 (2C), 123.59 (2C), 118.03 (2C), 117.98 (2C), 109.78, 102.61, 100.76, 88.94, 83.23, 82.71, 78.58, 77.02, 74.02, 67.27, 63.42, 60.07, 58.70, 58.37, 48.18, 47.87, 45.76, 43.53, 31.46 (2C); HRMS (ESI+) *m*/*z* calcd for $C_{37}H_{43}F_3N_5O_{13}$ [M + H] 822.2809, found 822.2838.

(2*S*,3*S*,4*S*)-2-((*R*)-2-Amino-1-((3a*R*,4*S*,6*R*,6a*R*)-6-(2,4-dioxo-3,4-dihydropyrimidin-1(2*H*)-yl)-2,2-dimethyltetrahydrofuro[3,4-*d*][1,3]dioxol-4-yl)-2-oxoethoxy)-6-((4-(4-(4-(trifluoromethoxy)phenoxy)piperidin-1-yl)benzyl)carbamoyl)-3,4-dihydro-2*H*-pyran-3,4-diyl diacetate (36).

To a stirred solution of **31** (27 mg, 0.047 mmol), **34** (52 mg, 0.14 mmol), HOBt (19 mg, 0.14 mmol) and NMM (52 μL, 0.47 mmol) in DMF (0.24 mL) was added EDCI (45 mg, 0.24 mmol). After being stirred for 11h at r.t., the reaction was quenched with aq.$NaHCO_3$, and extracted with $CHCl_3$/MeOH (9/1). The combined organic extracts were dried over Na_2SO_4 and concentrated *in vacuo*. The crude product was purified by silica gel column chromatography ($CHCl_3$/MeOH = 95/5) to afford **36** (37 mg, 84%): ^{1}H NMR (400 MHz, Methanol-d_4) δ 7.69 (d, *J* = 8.1 Hz, 1H), 7.20 (t, *J* = 9.5 Hz, 4H), 7.02 (d, *J* = 9.2 Hz, 2H), 6.98 (d, *J* = 8.5 Hz, 2H), 5.99 (t, *J* = 2.0 Hz, 1H), 5.87 (d, *J* = 3.0 Hz, 1H), 5.83 (d, *J* = 8.1 Hz, 1H), 5.66 (dd, *J* = 4.4, 2.5 Hz, 1H), 5.57 – 5.54 (m, 1H), 5.41 (d, *J* = 3.0 Hz, 1H), 4.78 (d, *J* = 2.3 Hz, 1H), 4.70 (dd, *J* = 6.3, 3.1 Hz, 1H), 4.63 (dd, *J* = 6.4, 3.5 Hz, 1H), 4.57 – 4.52 (m, 1H), 4.39 (s, 2H), 3.79 (t, *J* = 6.5 Hz, 1H), 3.64 (s, 1H), 3.49 (ddd, *J* = 10.9, 6.4, 3.6 Hz, 2H), 3.09 (ddd, *J* = 12.4, 8.6, 3.4 Hz, 2H), 2.83 (t, *J* = 6.5 Hz, 1H), 2.16 – 2.09 (m, 2H), 2.08 (s, 3H), 2.05 (s, 3H), 1.87 (dtd, *J* = 12.1, 8.1, 3.5 Hz, 2H), 1.53 (s, 3H), 1.21 (s, 3H); ^{13}C NMR (101 MHz, MeOD) δ 172.59, 171.76, 171.36, 166.16, 162.38, 157.61, 152.04, 151.92, 145.03, 142.46, 130.80, 129.66 (2C), 123.59 (2C), 118.05 (2C), 118.02 (2C), 115.67, 106.20, 103.33, 98.57, 92.78, 86.55, 85.61, 81.72, 77.88, 73.99, 64.84, 64.58, 61.28, 48.20

(2C), 43.59, 31.47 (2C), 27.52, 25.45, 20.66, 20.51; HRMS (ESI+) *m*/*z* calcd for $C_{42}H_{47}F_3N_5O_{15}$ [M + H] 918.3021, found 918.3053.

(2*S*,3*S*,4*S*)-2-((1*R*)-2-Amino-1-((2*S*,5*R*)-5-(2,4-dioxo-3,4-dihydropyrimidin-1(2*H*)-yl)-3,4-dihydroxytetrahydrofuran-2-yl)-2-oxoethoxy)-3,4-dihydroxy-*N*-(4-(4-(4-(trifluoromethoxy)phenoxy)piperidin-1-yl)benzyl)-3,4-dihydro-2*H*-pyran-6-carboxamide (8).

A solution of **35** (37 mg, 0.040 mmol) in a 4:1 mixture of TFA and H_2O (0.80 mL) was stirred for 4h at r.t., and concentrated *in vacuo*. A solution of the crude alcohol in a 5:1 mixture of MeOH and Et_3N (0.80 mL) was stirred for 10h at r.t., and concentrated *in vacuo*. The crude mixture was purified by reverse-phase HPLC [column: Luna® (C18, 10 μm, 100 Å, 250 × 10 mm), solvents: 35:65 MeOH:H_2O, flow rate: 3.0 mL/min, UV: 254 nm, retention time: 15 min] to afford DM-CPPB (**8**, 29 mg, 91%): ^{1}H NMR (400 MHz, Methanol-d_4) δ 7.92 (d, *J* = 8.1 Hz, 1H), 7.20 (d, *J* = 3.1 Hz, 2H), 7.18 (d, *J* = 3.5 Hz, 2H), 7.02 (d, *J* = 9.1 Hz, 2H), 6.96 (d, *J* = 8.6 Hz, 2H), 6.01 (d, *J* = 4.4 Hz, 1H), 5.80 (d, *J* = 3.0 Hz, 1H), 5.73 (d, *J* = 8.1 Hz, 1H), 5.14 (d, *J* = 6.7 Hz, 1H), 4.66 (d, *J* = 1.8 Hz, 1H), 4.57 – 4.51 (m, 1H), 4.50 (dd, *J* = 6.7, 1.7 Hz, 1H), 4.41 – 4.31 (m, 3H), 4.16 (dd, *J* = 6.6, 5.0 Hz, 1H), 4.04 (dd, *J* = 4.9, 3.0 Hz, 1H), 3.88 (dd, *J* = 6.7, 4.5 Hz, 1H), 3.47 (t, *J* = 6.2 Hz, 2H), 3.27 (d, *J* = 7.2 Hz, 1H), 3.07 (ddd, *J* = 17.0, 8.1, 4.0 Hz, 2H), 2.37 – 2.29 (m, 1H), 2.16 – 2.07 (m, 2H), 1.86 (dtd, *J* = 12.3, 8.2, 3.5 Hz, 2H); ^{13}C NMR (101 MHz, MeOD) δ 174.07, 170.14, 166.22, 163.14, 157.62, 152.12, 151.99, 144.89, 141.84, 131.07, 129.64 (2C), 123.58 (2C), 118.08 (2C), 118.03 (2C), 116.78, 108.52, 102.45, 101.32, 91.15, 84.20, 78.81, 75.49, 74.02, 71.19, 69.27, 63.69, 60.09, 47.81 (2C), 31.46 (2C); HRMS (ESI+) *m*/*z* calcd for $C_{35}H_{39}F_3N_5O_{13}$ [M + H] 794.2496, found 794.2522.

(2*R*)-2-(((2*S*,3*S*,4*S*)-3,4-Dihydroxy-6-(((4-(4-(4-(trifluoromethoxy)phenoxy)piperidin-1-yl)benzyl)amino)methyl)-3,4-dihydro-2*H*-pyran-2-yl)oxy)-2-((2*S*,5*R*)-5-(2,4-dioxo-3,4-dihydropyrimidin-1(2*H*)-yl)-4-hydroxy-3-methoxytetrahydrofuran-2-yl)acetamide (9).

To a stirred solution of **16** (5.8 mg, 0.0092 mmol) and DMSO (0.065 mL, 0.92 mmol) in a 5:1 mixture of CH_2Cl_2 and Et_3N (0.5 mL) was added SO_3•pyridine (15 mg, 0.092 mmol). After being stirred for 2h at r.t., the reaction mixture was added H_2O (0.1 mL) and passed through a silica gel pad ($CHCl_3$/MeOH = 93/7) to afford the crude **17**: this was used without purification. To a stirred solution of the crude **17** and **34** (17 mg, 0.046 mmol) in CH_3CN (0.5 mL) was added NaB(CN)H_3 (5.8 mg, 0.092 mol). After being stirred for 3h at r.t., the reaction was quenched with aq.$NaHCO_3$, and extracted with $CHCl_3$/MeOH (9/1). The combined organic extracts were dried over Na_2SO_4 and concentrated *in vacuo*. The crude product was passed through a silica gel pad ($CHCl_3$/MeOH = 9/1). The solution of the crude product in a 5:1 mixture of MeOH and Et_3N (0.5 mL) was stirred for 8h at r.t., and concentrated *in vacuo*. The crude mixture was purified by reverse-phase HPLC [column: Luna® (C18, 10 μm, 100 Å, 250 × 10 mm), solvents: 65:35 MeOH:H_2O, flow rate: 3.0 mL/min, UV: 254 nm, retention time: 15 min] to afford CPPA (**9**, 4.6 mg, 65% for 3 steps): ^{1}H NMR (400 MHz, Methanol-d_4) δ 8.02 (d, *J* = 8.1 Hz, 1H), 7.24 (d, *J* = 8.5 Hz, 2H), 7.19 (d, *J* = 8.5 Hz, 2H), 7.03 (d, *J* = 8.9 Hz, 2H), 6.99 (d, *J* = 8.5 Hz, 2H), 5.90 (d, *J* = 5.4 Hz, 1H), 5.76 (d, *J* = 7.8 Hz, 1H), 5.73 (d, *J* = 8.1 Hz, 1H), 5.06 (d, *J* = 6.6 Hz, 1H), 4.57 (dd, *J* = 6.4, 3.0 Hz, 1H), 4.52 (td, *J* = 4.4, 1.7 Hz, 1H), 4.33 (t, *J* = 5.2 Hz, 1H), 4.26 (d, *J* = 26.3 Hz, 1H), 4.18 (d, *J* = 1.6 Hz, 1H), 3.90 – 3.77 (m, 3H), 3.55 – 3.50 (m, 2H), 3.49 (s, 3H), 3.15 –

3.06 (m, 3H), 2.16 – 2.07 (m, 3H), 1.86 (m, *J* = 8.8, 4.3 Hz, 3H); ^{13}C NMR (101 MHz, MeOD) δ 174.07, 165.86, 163.68, 157.58, 151.26, 144.88, 142.07, 131.25, 129.37 (2C), 123.22 (2C), 118.03 (4C), 109.57, 102.60, 100.40, 90.92, 83.37, 80.46, 77.56, 74.63, 73.77, 73.15, 67.78, 63.30, 58.33, 48.19 (2C), 43.21, 30.74 (2C); HRMS (ESI+) *m*/*z* calcd for $C_{36}H_{43}N_3F_5O_{12}$ [M + H] 794.2860, found 794.2877.

(2*R*)-2-(((2*S*,3*S*,4*S*)-3,4-Dihydroxy-6-(((4-(4-(4-(trifluoromethoxy)phenoxy)piperidin-1-yl)benzyl)amino)methyl)-3,4-dihydro-2*H*-pyran-2-yl)oxy)-2-((2*S*,5*R*)-5-(2,4-dioxo-3,4-dihydropyrimidin-1(2*H*)-yl)-3-hydroxy-4-methoxytetrahydrofuran-2-yl)acetamide (10).

To a stirred solution of **26** (4.6 mg, 0.0073 mmol) and DMSO (0.052 mL, 0.73 mmol) in a 5:1 mixture of CH_2Cl_2 and Et_3N (0.5 mL) was added SO_3•pyridine (12 mg, 0.073 mmol). After being stirred for 2h at r.t., the reaction mixture was added H_2O (0.1 mL) and passed through a silica gel pad ($CHCl_3$/MeOH = 93/7) to afford the crude **29**. To a stirred solution of the crude **29** and **34** (13 mg, 0.036 mmol) in CH_3CN (0.5 mL) was added $NaB(CN)H_3$ (4.6 mg, 0.073 mol). After being stirred for 3h at r.t., the reaction was quenched with aq.$NaHCO_3$, and extracted with $CHCl_3$/MeOH (9/1). The combined organic extracts were dried over Na_2SO_4 and concentrated *in vacuo*. The crude product was passed through a silica gel pad ($CHCl_3$/MeOH = 9/1). A solution of the crude product in a 5:1 mixture of MeOH and Et_3N (0.5 mL) was stirred for 8h at r.t., and concentrated *in vacuo*. The crude mixture was purified by reverse-phase HPLC [column: Luna® (C18, 10 μm, 100 Å, 250 × 10 mm), solvents: 65:35 MeOH:H_2O, flow rate: 3.0 mL/min, UV: 254 nm, retention time: 15 min] to afford I-CPPA (**10**, 3.6 mg, 63% for 3 steps): ^{1}H NMR (400 MHz, Methanol-d_4) δ 8.04 (d, *J* = 8.1 Hz, 1H), 7.23 (d, *J* = 8.4 Hz, 2H), 7.19 (d, *J* = 8.7 Hz, 2H), 7.03 (d, *J* = 9.1 Hz, 2H), 6.98 (d, *J* = 8.5 Hz, 2H), 5.94 (d, *J* = 3.6 Hz, 1H), 5.74 (d, *J* = 8.1 Hz, 1H), 5.72 (d, *J* = 8.1 Hz, 1H), 5.06 (s, 1H), 4.59 – 4.52 (m, 2H), 4.43 – 4.38 (m, 1H), 4.28 (t, *J* = 5.4 Hz, 1H), 4.25 (t, *J* = 4.4 Hz, 1H), 4.21 (d, *J* = 1.5 Hz, 1H), 4.14 (dd, *J* = 8.3, 4.9 Hz, 1H), 3.88 – 3.85 (m, 2H), 3.82 (d, *J* = 8.2 Hz, 2H), 3.53 (s, 3H), 3.13 (ddd, *J* = 12.3, 8.7, 3.3 Hz, 2H), 2.11 (d, *J* = 9.7 Hz, 3H), 1.87 (ddt, *J* = 13.3, 8.9, 4.1 Hz, 3H); ^{13}C NMR (101 MHz, MeOD) δ 173.92, 165.98, 162.46, 157.87, 151.93, 143.90, 140.73, 130.53, 129.43 (2C), 123.29 (2C), 118.10 (2C), 117.87 (2C), 109.98, 103.08, 100.53, 91.27, 83.47, 80.53, 78.03, 74.70, 73.54, 67.84, 63.75, 58.42, 57.46, 48.20, 43.48 (2C), 31.49 (2C); HRMS (ESI+) *m*/*z* calcd for $C_{36}H_{43}N_3F_5O_{12}$ [M + H] 794.2860, found 794.2885.

(2*S*,3*S*,4*S*)-2-((1*R*)-2-Amino-1-((2*S*,5*R*)-5-(2,4-dioxo-3,4-dihydropyrimidin-1(2*H*)-yl)-4-hydroxy-3-methoxytetrahydrofuran-2-yl)-2-oxoethoxy)-3,4-dihydroxy-3,4-dihydro-2H-pyran-6-carboxylic acid (A-500359F).

A solution of **32** (18 mg, 29 μmol) in a 5:1 mixture of MeOH and Et_3N (0.5 mL) was stirred for 5h at r.t., and concentrated *in vacuo*. The crude mixture was purified by reverse-phase HPLC [column: Luna® (C18, 10 μm, 100 Å, 250 × 10 mm), solvents: 15:85 MeOH:H_2O, flow rate: 3.0 mL/min, UV: 254 nm, retention time: 14 min] to afford A-500359F (12 mg, 96%): ^{1}H NMR (400 MHz, Deuterium Oxide) δ 7.75 (d, *J* = 8.1 Hz, 1H), 5.88 (d, *J* = 8.1 Hz, 1H), 5.80 (dd, *J* = 2.5, 1.6 Hz, 1H), 5.78 (d, *J* = 4.0 Hz, 1H), 5.25 (d, *J* = 3.2 Hz, 1H), 4.71 (d, *J* = 2.1 Hz, 1H), 4.48 (dd, *J* = 5.7, 2.1 Hz, 1H), 4.43 (dd, *J* = 4.5, 2.5 Hz, 1H), 4.30 (dd, *J* = 5.1, 4.0 Hz, 1H), 4.12 (ddd, *J* = 4.8, 3.3, 1.7 Hz, 1H), 3.73 (t, *J* = 5.4 Hz, 1H), 3.35 (s, 3H); ^{13}C NMR (101 MHz, D_2O) δ 173.32, 168.26, 166.06, 151.29, 144.11, 140.79,

108.44, 101.93, 98.62, 89.42, 81.99, 78.20, 75.00, 72.10, 64.43, 62.19, 57.93; HRMS (ESI+) *m*/*z* calcd for $C_{17}H_{22}N_3O_{12}$ [M + H] 460.1204, found 460.1215.

Synthesis of CPPB (5) in Scheme 4.

To a stirred solution of A-500359F (11 mg, 0.024 mmol), **34** (26 mg, 0.072 mmol), Glyceroacetonide-Oxyma (16 mg, 0.072 mmol)[54] and NMM (26 mL, 0.24 mmol) in DMF (0.49 mL) was added EDCI (23 mg, 0.12 mmol). After being stirred for 5h at r.t., the reaction mixture was filtered, and diluted with water. The product was extracted with $CHCl_3$/MeOH (9/1). The combined extracts were derived over Na_2SO_4, and concentrated *in vacuo*. The crude mixture was purified by DOWEX 50Wx4 (MeOH : NH_4OH = 4 : 1) followed by reverse-phase HPLC [column: Luna (C_{18}, 10 mm, 100 Å, 250 × 10 mm), solvents: 65:35 MeOH : H_2O, flow rate: 3.0 mL/min, UV: 254 nm, retention time: 18 min] to afford **5** (17 mg, 92%). All physical data were identical to that of CPPB synthesized in Scheme 3A.

Expression and purification of *Hy*MraY.

The gene *mraY* of *Hydrogenivirga spp.* 128–5-R1–1 was cloned with a *N*-terminal His_6 tag into a pET22b vector. The plasmid was transformed and expressed in *E. coli* NiCo21(DE3) pLEMO competent cells. The proteins were purified using a nickel, cation exchange, and size exclusion chromatography. The final storage buffer was 20 mM HEPES pH 7.5, 100 mM NaCl, 10% glycerol, 5 mM βME, 0.15% decyl β-D-maltopyranoside (DM).

Expression and purification of *Mj*AglH.

The gene *mj1113* of *Methanocaldococcus jannaschii* DSM 2661 was cloned with a *N*-terminal His_9 tag into a pET33b-derived vector. The plasmid was transformed and expressed in *E. coli* NiCo21(DE3) pLEMO competent cells. The proteins were purified using cobalt and size exclusion chromatography. The final storage buffer was 20 mM Tris-HCl, pH 7.5, 100 mM NaCl, 5% glycerol, 5 mM βME, 0.15% DM.

Preparation of membrane fraction P-60 containing WecA.

E. coli B21 wecA strain were harvested by centrifugation (4,700 rpm) at 4 °C followed by washing with 0.9% saline solution (thrice).[9,58] The washed cell pellets were washed with homogenization buffer (containing 50 mM K_2HPO_4, 5 mM $MgCl_2$, 5 mM 1,4-dithio-DL-threitol, and 10% glycerol, pH = 7.2) (thrice), and approximately 5 g of pellet (wet weight) was collected. The washed cell pellets were suspended in homogenization buffer and disrupted by probe sonication on ice (5sec on and 2sec off for 1 min, then cool down for 1.5min, 5 cycles, cool down for 15min, and then, 5sec on and 2sec off for 1min, cool down for 1.5min, 5 cycles). The resulting suspension was centrifuged at 4,700 xg for 15min at 4 °C to remove unbroken cells. The lysate was centrifuged at 25,000 xg for 20min. at 4 °C. The supernatant was subjected to ultracentrifugation at 60,000 xg for 1h at 4 °C. The supernatant was discarded, and the membrane fraction containing WecA enzyme (P-60) was suspended in the Tris-HCl buffer (pH = 7.5). Total protein concentrations were approximately 8 to 10 mg/mL. Aliquots were stored in Eppendorf tubes at -80 °C.

DPAGT1 expression and purification.

DPAGT1 was expressed in suspended Expi293 cells for 36h. The cells were lysed by drawing through a 26g needle (10 times) and membrane protein was extracted using buffer containing 1% decyl β-D-maltopyranoside detergent. DPAGT1 was purified using HA-agarose resin and a superdex 200 size exclusion column.

MraY assay.

MraY assay substrates, Park's nucleotide-N^e-C_6-dansylthiourea, neryl phosphate, were chemically synthesized according to the reported procedures.[7] Park's nucleotide-N^e-C_6-dansylthiourea (2 mM stock solution, 1.88 μL), $MgCl_2$ (0.5 M, 5 μL), KCl (2 M, 5 μL), Triton X100 (0.5%, 5.63 μL), Tris-HCl buffer (pH 8.0, 50 mM), neryl phosphate (0.1 M, 2.25 μL), and inhibitor molecule (0 – 50 μg/mL in Tris-HCl buffer) were placed in a 1.5 mL Eppendorf tube. To a reaction mixture, P-60 (10μL) was added (total volume of reaction mixture: 50 μL adjust with Tris-HCl buffer). The reaction mixture was incubated for 2h at r.t. (26 °C) and quenched with $CHCl_3$ (100 μL). Two phases were mixed via vortex and centrifuged at 25,000 xg for 10min. The aqueous phase was assayed via reverse-phase HPLC. The water phase (10 μL) was injected into HPLC (solvent: CH_3CN/0.05 M aq. NH_4HCO_3 = 25:75; UV: 350 nm; flow rate: 0.5 mL/min; column: Kinetex 5μm C8, 100 A, 150 × 4.60 mm), and the area of the peak for lipid I-neryl derivative was quantified to obtain the IC_{50} value. The IC_{50} values were calculated from plots of the percentage product inhibition versus the inhibitor.

WecA assay.

WecA assay substrate, UDP-Glucosamine-C_6-FITC was chemically synthesized according to the reported procedures.[9,11,59] UDP-Glucosamine-C_6-FITC (UDP-GlcN-C_6-FITC, 2 mM stock solution, 0.56 μL), $MgCl_2$ (0.5 M, 4 μL), β-mercaptoethanol (50 mM, 5 μL), CHAPS (5%, 11.3 μL), Tris-HCl buffer (pH 8.0, 50 mM), undecaprenyl phosphate (4 mM, 1.4 μL), and inhibitor molecue (0 – 50 μg/mL in Tris-HCl buffer) were place in a 1.5 μL Eppendorf tube. To a reaction mixture, P-60 (10 μL) was added (total volume of reaction mixture: 50 μL adjust with Tris-HCl buffer). The reaction mixture was incubated for 2h at 37 °C and quenched with n-butanol (150 μL). Two phases were mixed via vortex and centrifuged at 10,000 xg for 3min. The upper organic phase was assayed via reverse-phase HPLC. The organic phase (30 μL) was injected into HPLC (solvent: gradient elution of 85:15 to 95:5 MeOH/0.05 M aq. NH_4HCO_3; UV: 485 nm; flow rate: 0.5 ml/ min; column: Kinetex 5 μm C8, 100 Å, 150 × 4.60 mm), and the area of the peak for C_{55}-P-P-GlcN-C_6-FITC was quantified to obtain the IC_{50} value. The IC_{50} values were calculated from plots of the percentage product inhibition versus the inhibitor concentration.

AglH assay.

AglH assays were performed as the procedure described for WecA assays, but used *Mj*AglH and α-dihydroundecaprenyl phosphate (C_{55}-dolichyl phosphate) instead of WecA and undecaprenyl phosphate. UDP-GlcN-C_6-FITC (2 mM stock solution, 0.56 μL), $MgCl_2$ (0.5 M, 4 μL), β-mercaptoethanol (50 mM, 5 μL), CHAPS (5%, 11.3 μL), Tris-HCl buffer (pH 8.0, 50 mM), C_{55}-dolichyl phosphate (4 mM, 1.4 μL), and inhibitor molecule (0 – 50 μg/mL

in Tris-HCl buffer) were place in a 1.5 μL Eppendorf tube. To a reaction mixture, AglH solution (10 μL) was added (total volume of reaction mixture: 50 μL adjust with Tris-HCl buffer). The reaction mixture was incubated for 2h at 37 °C and quenched with n-butanol (150 μL). Two phases were mixed via vortex and centrifuged at 10,000 xg for 3min. The upper organic phase was assayed via reverse-phase HPLC. The organic phase (30 μL) was injected into HPLC (solvent: gradient elution of 85:15 to 95:5 MeOH/0.05 M aq. NH_4HCO_3; UV: 485 nm; flow rate: 0.5 ml/ min; column: Kinetex 5 μm C8, 100 Å, 150 × 4.60 mm), and the area of the peak for C_{55}-P-P-GlcN-C_6-FITC was quantified to obtain the IC_{50} value. The IC_{50} values were calculated from plots of the percentage product inhibition versus the inhibitor concentration.

DPAGT1 assay.

DPAGT1 assays were performed as the procedure described for AglH assays, but used DPAGT1.

Cell lines.

The human primary PDAC cell lines PANC-1 (ATCC CRL 1469); Capan-2 (ATCC HTB-80) and metastatic PDAC cell lines Capan-1 (ATCC HTB-79), AsPC-1 (ATCC CRL-1682), L1210 (ATCC CCL-219), KB (ATCC CCL-17), HeLa, SiHa (ATCC HTB-35), HCT-116 (ATCC CCL-247), DLD-1 (ATCC CCL221), hTERT-HPNE (ATCC CRL-4023), Vero (ATCC CCL-81) were purchased from the ATCC. The cell lines were cultured and maintained in the media as recommended by the supplier. The cell lines were regularly tested for mycoplasma contamination and authenticated. In addition to ATCC cell lines, Dr. Glazer's lab generated patient-derived PDAC cell line, PD002. PD002 Cells were maintained and cultured in DMEM medium supplemented with 20% FBS and 100 IU/mL penicillin and incubated at 37°C with 5% CO_2.

MTT cytotoxicity assay.

To study the effect of treatment with DPAGT1 inhibitors on the growth and proliferation of cells, a fixed number of cells (5×10^4 cells/well, 196 μL) were plated in a 96 well plate. Into each well 5 μL of drug concentration was added. After 72h of incubation with drugs at 37 °C, 5% CO_2, 10 μL of MTT solution (5 mg/mL in PBS) was added and incubated another 3h at 37 °C, 5% CO_2. The medium was removed, and DMSO (200 μL/well) was added. Viability was assessed on the basis of cellular conversion of MTT into a purple formazan product. The absorbance of the colored formazan product was measured at 570 nm by BioTek Synergy HT Spectrophotometer.

Kinetic proliferation assay.

To study the effect of treatment with DPAGT1 inhibitors on the growth and proliferation of cells, a fixed number of cells (2×10^4) were plated in multiple wells of a 96 well plate, incubated for 24h to let cells settle down. Then, CPPB (**5**) was added (0–50 μM). Images were obtained every 4h using an IncuCyte Live-Cell Imaging System (Essen BioScience, Ann Arbor, MI). After 72h, cell proliferation was quantified using the metric phase object

confluence (POC), a measurement of the area of the field of view that is covered by cells, which is calculated by the integrated software.

Scratch assay.

A confluent monolayer was formed in 24-well plates. The monolayer was scratched by a sterile 200 μL pipette tip and washed with PBS to remove cell debris. Complete medium with CPPB (**5**) (0, 0.05, 0.1, 0.2 μM) were added and scratched areas were photographed with microscope. The scratched cells were incubated at 37 °C, 5% CO_2. After 24h, medium was removed and cells were stained with a 1:1 mixture of crystal violet and PBS for 5min, washed with PBS twice, and photographed with microscope. Wound areas were measured and recovered areas were calculated.

Cell migration assays using transwell chamber.

Cell migration assay was performed using Boyden chamber (Thermo Fisher). PD002 cells (~10^4 cells/mL) were seeded in 96-wells plate (Corning, HTS Transwell-96 Well Permeable Supports, pore size: 8 μm) in FBS free media and the lower chambers were filled with 10% FBS medium. CPPB, tunicamycin, or gemcitabine (0.1 μM) was added to the upper chamber. The cells were incubated for 18h at 37°C under 5% CO_2. The cells were fixed using 4% paraformaldehyde for 0.5h and stained with 0.05% crystal violet (300 μL/well), after 0.5h, images were captured via 10X magnification microscopy.

Reagents, antibodies, and cell treatments.

All the primary and secondary antibodies used were obtained from Cell Signaling Technology.

SDS-PAGE and Western blotting assay.

The medium of the cells grown in 10 cm cell culture plate was removed, and the cells were washed once with PBS, and lysed with Pierce RIPA buffer (Theomo Scientific, Cat. # 89901) containing 1x Pierce protease and phosphatase inhibitors (Thermo Scientific, Cat. # 88668). The cell lysate was pelleted down at 15,200 xg at 4 °C for 15min, the cell supernatant was transferred to a fresh Eppendorf tube, and 5 uL of sample was quantitated by using (Quick Start Bradford Dyed Reagent, Biorad, Cat. # 500–0205). 50 μg of each protein sample was analyzed by SDS-PAGE (10% gel) followed by Western blotting, and autoradiography. Precision Plus Dual Color (Biorad, Cat. # 161–0374) was used as protein standard marker. Clarity Western ECL Substrate (Biorad, Cat. # 170–5060) was used to develop the probe signal, and Classic Blue BX film (MidSci, Ref. # 604 5983) was used for autoradiography.

Immunofluorescent staining.

A confluent monolayer was formed in Nunc™ Lab-Tek™ II CC2™ chamber slide (8 well, Thermo Scientific, Cat. # 154941PK). Complete medium with CPPB (**5**, 0–20 μM) was added and incubated at 37 °C under 5% CO_2. After 24h, medium was removed and cells were washed with PBS (3 times), then fixed with 4% paraformaldehyde in PBS for 0.5h at 4 °C. After washing with 0.2% Tween-20/PBS (3 times), the cells were treated with a blocking

buffer (0.2% Tween-20, 1% NGS, 1% BSA in PBS) for 2h at 4 °C. The cells were treated with primary antibody in blocking buffer (0.4% v/v) for 12h at 4 °C. The cells were washed with 0.2% Tween-20 in PBS (3 times) and treated with secondary antibody (Donkey anti-Rabbit IgG (H+L) Highly Cross-Adsorbed Secondary Antibody, Alexa Fluor 555 (Invitrogen, Cat. # A31572)) in blocking buffer (0.2% v/v) for 2h at r.t. in the dark. After additional washing (3 times) with 0.2% Tween-20/PBS, the cells were treated with DAPI Fluoromount-G® (SouthernBiotech, Cat. # 0100–20) and covered with glass slide for fluorescence microscopy analysis.

Reverse transcription-quantitative polymerase chain reaction (RT-qPCR).

Total RNA was extracted from PD002 (~10^6) cells using a RNeasy Mini kit (Qiagen, Inc., Valencia, CA, USA) after the treatment with CPPB or tunicamycin (0–10 μM) for 24h. Expression was measured by Kapa probe fast qPCR Master Mix (2X) (KAPA BIOSYSTEMS; Wilmington, MA, USA) with S19 as an endogenous control. Primer sequences were as follow; *DPAGT1*, forward, 5'-tcagggacaaagagatctgga-3'; reverse, 5'-cagcatggtttgttctaatgctt-3'. The PCR cycling conditions were performed with total 45 cycles at 95 °C for 10sec and 60 °C for 10sec, 72 °C for 10sec, and cooled down at 40 °C for 30sec. Relative mRNA expression changes were calculated by the 2-ΔΔCq method.

Synergistic effect of CPPB with paclitaxel.

The synergistic or antagonistic activities of CPPB (**5**) with paclitaxel were assessed *in vitro* via micro dilution broth checkerboard technique.[48] PD002 cells (180 μL, 1×10^4/mL) were places in each well of a 96well plate. The cells were treated with a combination of CPPB (0–50 μM) and paclitaxel (5–0.024 μM), and cultured at 37 °C for 72h under 5% CO_2. Antiproliferation kinetic of each well were monitored by using an IncuCyte Live-Cell Imaging System (Essen BioScience, Ann Arbor, MI). At the endpoint, MTT assays were performed. The FIC index was calculated according to the following equation. $\Sigma FIC=FIC_A+FIC_B=C_A/MIC_A+C_B/MIC_B$ where, MIC_A and MIC_B: MIC of drugs A and B, C_A and C_B=concentrations of drugs A and B used in combination. In these interaction studies, ΣFIC of less than 0.5 represents synergistic activity.

Computational methods – DPAGT1 inhibitor study.

Protein preparation: All molecular modeling and docking studies were performed using the experimental structure of the human GPT (DPAGT1, H129 variant) with bound tunicamycin (PDB 6BW6).[25] The biological unit was downloaded and prepared using the Protein Preparation Wizard of the Maestro Small Molecule Drug Discovery Suite (Schrödinger, LLC).[49] Hydrogens were added, when applicable, and protonation and tautomeric states were assigned using the Epic program.[60] Lone waters were removed and the protein was refined by optimizing H-bond assignments and performing a restrained minimization using MacroModel.[50] Docking site preparation: The docking receptor grid was prepared using Schrödinger's Glide program.[51,61] The docking grid was defined as 25 Å region centroid of the bound tunicamycin compound. Van der Waals radius scaling was employed with a scaling factor of 1.0 and partial charge cutoff of 0.25 (default values). No docking constraints or excluded volumes were defined. Hydroxyl and thiol groups within close

proximity to the bound tunicamycin compound (≤ 3Å) were defined as rotatable. Inhibitor docking: Compounds were built and prepared for docking using the LigPrep program using default settings (Schrödinger, LLC). The DPAGT1 inhibitors, non-inhibitors, and weak inhibitor reported herein were docked into the prepared protein using Schrödinger's Glide program using XP (extra precision) settings using the grid described above.[62] Glide XP score for CPPB (**5**), I-CPPB (**6**), CPPA (**9**), I-CPPA (**10**), OM-CPPB (**7**), DM-CPPB (**8**), I-CAP (**10**), OM-CAP (**2**), and CAP (**1**) are summarized in Table S1 in Supporting Information.

Supplementary Material

Refer to Web version on PubMed Central for supplementary material.

ACKNOWLEDGMENTS

Research reported in this publication was supported by the National Institute of General Medical Sciences of the National Institutes of Health under award number R01GM114611. M.K. thanks UTRF (University of Tennessee Health Science Center) for generous financial support (Innovation award R079700292). NMR data were obtained on instruments supported by the NIH Shared Instrumentation Grant. M.K. would like to thank Dr. Michael McNeil (Colorado State University) for providing *E. coli* B21 WecA strain. The authors gratefully acknowledge Miss Shakiba Eslamimehr and Mr. David Mingle for their efforts in culturing several cancer call lines used in this article.

Funding Sources

NIH/GM114611

ABBREVIATIONS

THF	tetrahydrofuran
CH_2Cl_2	methylene chloride
DMSO	dimethyl sulfoxide
DMF	*N*,*N*-dimethylformamide
MeOH	methanol
EtOH	ethanol
iPrOH	isopropanol
tBuOH	*tert*-butanol
EtOAc	ethyl acetate
$CHCl_3$	chloroform
HRMS	high resolution mass spectrometry
HPLC	high performance liquid chromatography
TLC	thin layer chromatography
Bu	*n*-butyl

Ts	*p*-toluenesulfonyl
DMAP	*N*,*N*-dimethyl-4-aminopyridine
Boc	*tert*-butoxycarbonyl
EDCI	1-(3-dimethylaminopropyl)-3-ethylcarbodiimide hydrochloride
AcOH	acetic acid
Et_3N	triethylamine
NIS	*N*-iodosuccinimide
TFA	2,2,2-trifluoroacetic acid
MS	molecular sieve
ATCC	American type culture collection
SAR	structure–activity relationship
MIC	minimum inhibitory concentration
FIC	fractional inhibitory concentration
MTT	3-(4,5-dimethylthiazol-2-yl)-2,5-diphenyltetrazolium bromide
OD	optical density
PBS	phosphate-buffered saline
FBS	fetal bovine serum
NADPH	nicotinamide adenine dinucleotide phosphate
UDP-GlcNAc	uridine diphosphate *N*-acetylglucosamine
UMP	uridine monophosphate
RT-qPCR	reverse transcription quantitative real time polymerase chain reaction
CAP	capuramycin
OM-CAP	*O*-methyl capuramycin
DM-CAP	demethyl capuramycin
CPPB	capuramycin phenoxypiperidinylbenzylamide
I-CPPB	*iso*-capuramycin phenoxypiperidinylbenzylamide
OM-CPPB	*O*-methyl capuramycin phenoxypiperidinylbenzylamide

DM-CPPB	demethyl capuramycin phenoxypiperidinylbenzylamide
CPPA	capuramycin phenoxypiperidinylbenzylamine
I-CPPA	*iso*-capuramycin phenoxypiperidinylbenzylamine

REFERENCES AND NOTES

(1). Siricilla S; Mitachi K; Wan B; Franzblau SG; Kurosu M Discovery of a capuramycin analog that kills nonreplicating Mycobacterium tuberculosis and its synergistic effects with translocase I inhibitors. J. Antibiot 2015, 68, 271–278. [PubMed: 25269459]

(2). Koga T; Fukuoka T; Harasaki T; Inoue H; Hotoda H; Kakuta M; Muramatsu Y; Yamamura N; Hoshi M; Hirota T Activity of capuramycin analogs against Mycobacterium tuberculosis, Mycobacterium avium and Mycobacterium intracellular in vitro and in vivo. J. Antimicro. Chemother 2004, 54, 755–760.

(3). Nikonenko BV; Reddy VM; Protopopova M; Bogatcheva E; Einck L; Nacy CA Activity of SQ641, a capuramycin analog, in a murine model of tuberculosis. Antimicrob. Agents Chemother 2009, 53, 3138–3139. [PubMed: 19414567]

(4). Kurosu M; Li K Synthetic studies towards the identification of novel capuramycin analogs with antimycobacterial activity. Heterocycles 2009, 77, 217–225.

(5). Reddy VM; Einck L; Nacy CA In vitro antimycobacterial activity of capuramycin analogs. Antimicro. Agents Chemother 2008, 52, 719–721.

(6). Moore JH; van Opstal E; Kolling GL; Shin JH; Bogatcheva E; Nikonenko B; Einck L; Phipps AJ; Guerrant RL; Protopopova M; Warren CA Treatment of Clostridium difficile infection using SQ641, a capuramycin analogue, increases post-treatment survival and improves clinical measures of disease in a murine model. J. Antimicrob Chemother 2016, 71, 1300–1306. [PubMed: 26832756]

(7). Siricilla S; Mitachi K; Skorupinska-Tudek K; Swiezewska E; Kurosu M Biosynthesis of a water-soluble lipid I analogue and a convenient assay for translocase I, Anal. Biochem 2014, 461, 36–45. [PubMed: 24939461]

(8). Mitachi K; Aleiwi BA; Schneider CM; Siricilla S; Kurosu M Stereocontrolled total synthesis of muraymycin D1 having a dual mode of action against Mycobacterium tuberculosis. J. Am. Chem. Soc 2016, 138, 12975–12980. [PubMed: 27617631]

(9). Mitachi K; Siricilla S; Yang D; Kong Y; Skorupinska-Tudek K; Swiezewska E; Franzblau SG; Kurosu M Fluorescence-based assay for polyprenyl phosphate-GlcNAc-1-phosphate transferase (WecA) and identification of novel antimycobacterial WecA inhibitors. Anal. Biochem 2016, 512, 78–90. [PubMed: 27530653]

(10). Kurosu M Structure-based drug discovery N-glycan biosynthesis, dolichyl-phosphate N-acetylglucosaminephosphotransferase. Future Med. Chem 2019, 11, 927–933. [PubMed: 30907628]

(11). Mitachi K; Kurosu SM; Gillman CD; Yun H-G; Clemons WM; Kurosu M A practical synthesis of a novel DPAGT1 inhibitor, aminouridyl phenoxypiperidinbenzyl butanamide (APPB) for in vivo studies. MethodsX 2019, 6, 2305–2321. [PubMed: 31667130]

(12). Mitachi K; Kurosu S; Eslamimehr S; Lemieux M; Ishizaki Y; Clemons W; Kurosu M A semi-synthesis of an anticancer DPAGT1 inhibitor from a muraymycin biosynthetic intermediate. Org. Lett 2019, 21, 876–879. [PubMed: 30698984]

(13). Mitachi K; Yun H-G; Kurosu SM; Eslamimehr S; Lemieux MR; Klaić L; Clemons WM; Kurosu M Novel FR-900493 analogs that inhibit outgrowth of Clostridium difficile spores. ACS Omega 2018, 3, 1726–1739. [PubMed: 29503973]

(14). Kurosu M Inhibition of N-glycosylation towards novel anti-cancer chemotherapeutics. J. Mol. Pharm. Org. Process Res 2018, 6, 141. [PubMed: 30417028]

(15). van Heijenoort J Lipid intermediates in the biosynthesis of bacterial peptidoglycan. Microbiol. Mol. Biol. Rev 2007, 71, 620–635. [PubMed: 18063720]

(16). Ishizaki Y; Hayashi C; Inoue K; Igarashi M; Takahashi Y; Pujari V; Crick DC; Brennan PB; Nomoto A Inhibition of the first step in synthesis of the mycobacterial cell wall core, catalyzed by the GlcNAc-1-phosphate transferase WecA, by the novel caprazaymicin derivative CPZEN-45. J. Biol. Chem 2013, 288, 30309–30319. [PubMed: 23986448]

(17). Zhong J-T; Yu J; Wang H-J; Shi Y; Zhao T-S; He B-X; Qiao B; Feng Z-W Effects of endoplasmic reticulum stress on the autophagy, apoptosis, and chemotherapy resistance of human breast cancer cells by regulating the PI3K/AKT/mTOR signaling pathway. Tumor Biol 2017, 39, 010428317697562.

(18). Morin MJ; Bernacki RJ Biochemical effects and therapeutic potential of tunicamycin in murine L1210 leukemia. Cancer Res 1983, 43, 1669–1674. [PubMed: 6339042]

(19). Price NPJ; Hartman TM; Li J; Velpula KK; Naumann TA; Guda MR; Yu B; Bischoff KM Modified tunicamycins with reduced eukaryotic toxicity that enhance the antibacterial activity of β-lactams. J. Antibiot 2017, 70, 1070–1077.

(20). Yamaguchi H; Sato S; Yoshida S; Takada K; Itoh M; Seto H; Otake N Capuramycin, a new nucleoside antibiotic. Taxonomy, fermentation, isolation and characterization. J. Antibiot 1986, 39, 1047–1053. [PubMed: 3759655]

(21). Bogatcheva E; Dubuisson T; Protopopova M; Einck L; Nacy CA; Reddy VM Chemical modification of capuramycins to enhance antibacterial activity. J. Antimicrob. Chemother 2011, 66, 578–587. [PubMed: 21186194]

(22). Kurosu M; Li K; Crick DC Concise synthesis of capuramycin. Org. Lett 2009, 11, 2393–2396. [PubMed: 19405507]

(23). Wang Y; Siricilla S; Aleiwi BA; Kurosu M Improved synthesis of capuramycin and its analogs. Chem. Eur. J 2013, 19, 13847–13858. [PubMed: 24014478]

(24). Bal BS; Childers WE; Pinnick HW Oxidation of α,β-unsaturated aldehydes. Tetrahedron 1981, 37, 2091–2096.

(25). Dong YY; Wang H; Pike ACW; Cochrane SA; Hamedzadeh S; Wyszyński FJ; Bushell SR; Royer SF; Widdick DA; Sajid A; Boshoff HI; Park Y; Lucas R; Liu WM; Lee SS; Machida T; Minall L; Mehmood S; Belaya K; Liu WW; Chu A; Shrestha L; Mukhopadhyay SMM; Strain-Damerell C; Chalk R; Burgess-Brown NA; Bibb MJ; Barry III CE; Robinson CV; Beeson D; Davis BG; Carpenter EP Structures of DPAGT1 explain glycosylation disease mechanisms and advance TB antibiotic design. Cell 2018, 175, 1045–1058. [PubMed: 30388443]

(26). Yoo J; Mashalidis EH; Kuk ACY; Yamamoto K; Kaeser B; Ichikawa S; Lee SY GlcNAc-1-P-transferase-tunicamycin complex structure reveals basis for inhibition of N-glycosylation. Nat. Struct. Mol. Biol 2018, 25, 217–224. [PubMed: 29459785]

(27). Blair HA; Scott LJ Delamanid: a review of its use in patients with multidrug-resistant tuberculosis. Drugs 2015, 75, 91–100. [PubMed: 25404020]

(28). Matsumoto M; Hashizume H; Tomishige T; Kawasaki M; Tsubouchi H; Sasaki H; Shimokawa Y; Komatsu M OPC-67683, a nitro-dihydro-imidazooxazole derivative with promising action against tuberculosis in vitro and in mice. PLoS Medicine 2006, 3, e466. [PubMed: 17132069]

(29). de-Freitas-Junior JCM; Bastos LG; Freire-Neto CA; Du Rocher B; Abdelhay ESFW; Morgado-Diaz JA N-glycan biosynthesis inhibitors induce in vitro anticancer activity in colorectal cancer cells. J. Cell. Biochem 2012, 113, 2957–2966. [PubMed: 22552949]

(30). Belaya K; Finlayson S; Slater CR; Cossins J; Liu WW; Maxwell S; McGowan SJ; Maslau S; Twigg SRF; Walls TJ; Pascual PSI; Palace J; Beeson D Mutations in DPAGT1 cause a limb-girdle congenital myasthenic syndrome with tubular aggregates. Am. J. Hum. Gen 2012, 91, 193–201.

(31). Varelas X; Bouchie MP; Kukuruzinska MA Protein N-glycosylation in oral cancer: Dysregulated cellular networks among DPAGT1, E-cadherin adhesion and canonical Wnt signaling. Glycobiology 2014, 24, 579–591. [PubMed: 24742667]

(32). Nita-Lazar M;, Noonan V; Rebustini I; Walker J; Menko AS; Kukuruzinska MA Overexpression of DPAGT1 leads to aberrant N-glycosylation of E-cadherin and cellular discohesion in oral cancer. Can. Res 2009, 69, 5673–5680.

(33). Vargas DA; Sun M; Sadykov K; Kukuruzinska MA; Zaman MH The integrated role of Wnt/β-Catenin, N-glycosylation, and E-cadherin-mediated adhesion in network dynamics. PLoS Comp. Biol 2016, 12, e1005007/1–e1005007/26.

(34). Jamal B; Sengupta PK; Gao Z; Nita-Lazar M; Amin B; Jalisi S; Bouchie MP; Kukuruzinska MA Aberrant amplification of the crosstalk between canonical Wnt signaling and N-glycosylation gene DPAGT1 promotes oral cancer. Oral Oncol 2012, 48, 523–529. [PubMed: 22341307]

(35). Sengupta PK; Bouchie MP; Kukuruzinska MA N-Glycosylation gene DPAGT1 is a target of the Wnt/β-Catenin signaling pathway. J. Biol. Chem 2010, 285, 31164–31173. [PubMed: 20693288]

(36). Cory G Scratch-wound assay. Methods Mol. Biol 2011, 769, 25–30. [PubMed: 21748666]

(37). Gomez-Lopez N; Vadillo-Ortega F; Estrada-Gutierrez G Combined Boyden-flow cytometry assay improves quantification and provides phenotypification of leukocyte chemotaxis. PLoS ONE 2011, 6, e28771. [PubMed: 22174892]

(38). Doerr ME; Jones JI The roles of integrins and extracellular matrix proteins in the insulin-like growth factor I-stimulated chemotaxis of human breast cancer cells. J. Biol. Chem 1996, 271, 2443–2447. [PubMed: 8576205]

(39). Wu Y; Zhou BP Snail: More than EMT. Cell Adh. Migr 2010, 4, 199–203. [PubMed: 20168078]

(40). Wang Y; Shi J; Chai K; Ying X; Zhou BP The role of Snail in EMT and tumorigenesis. Curr. Cancer Drug. Targets 2013, 13, 963–972. [PubMed: 24168186]

(41). Barrallo-Gimeno A; Nieto MA The Snail genes as inducers of cell movement and survival: implications in development and cancer. Development 2005, 132, 3151–3161. [PubMed: 15983400]

(42). Vistain LF; Yamamoto N; Rathore R; Cha P; Meade TJ Targeted inhibition of Snail activity in breast cancer cells by using a Co(III)-Ebox conjugate. Chembiochem 2015, 16, 2065–2072. [PubMed: 26305708]

(43). Conroy T; Desseigne F; Ychou M; Bouche O; Guimbaud R; Becouarn Y; Adenis A; Raoul J-L; Gourgou-Bourgade S; de la Fouchardiere C; Bennouna J; Bachet J-B; Khemissa-Akouz F; Pere-Verge D; Delbaldo C; Assenat E; Chauffert B; Michel P; Montoto-Grillot C; Ducreux M FOLFIRINOX versus gemcitabine for metastatic pancreatic cancer. New Engl. J. Med 2011, 364, 1817–1825. [PubMed: 21561347]

(44). Rasmussen LS; Fristrup CW; Jensen BV; Pfeiffer P; Weber B; Yilmaz MK; Poulsen LO; Ladekarl M; Falkmer UG; Osterlind K; Larsen JS; Skuladottir H; Hansen CP; Mortensen MB; Mortensen FV; Sall M; Detlefsen S; Bogsted M Initial treatment and survival in 4163 Danish patients with pancreatic cancer: A nationwide unselected real-world register study. Eur. J. Cancer 2020, 129, 50–59.

(45). Chiorean EG; Cheung WY; Giordano G; Kim G; Al-Batran S-E. Real-world comparative effectiveness of nab-paclitaxel plus gemcitabine versus FOLFIRINOX in advanced pancreatic cancer: a systematic review. Ther. Adv. Med. Oncol 2019, 11, 1758835919850367. [PubMed: 31205510]

(46). Belli C; Cereda S; Reni M Role of taxanes in pancreatic cancer. World J. Gastroenterol 2012, 18, 4457–4465. [PubMed: 22969215]

(47). Mitachi K; Shajila S; Yang J; Eslamimehr S; Lemieux M R; Meibohm, B.; Ji, Y. Kurosu, M. A new combination of a pleuromutilin derivative and doxycycline for treatment of multidrug-resistant Acinetobacter baumannii. J. Med. Chem 2017, 60, 2869–2878. [PubMed: 28291943]

(48). Hsieh MH; Chen MY; Victor LY; Chow JW Synergy assessed by checkerboard. A critical analysis. Diagn. Microbiol. Infect. Dis 1993, 16, 343–349. [PubMed: 8495592]

(49). Schrödinger Release 2019–4: Maestro, Schrödinger, LLC, New York, NY, 2019.

(50). Schrödinger Release 2019–4: MacroModel, Schrödinger, LLC, New York, NY, 2019.

(51). Schrödinger Release 2019–4: LigPrep, Schrödinger, LLC, New York, NY, 2019.

(52). Hotoda H; Furukawa M; Daigo M; Murayama K; Kaneko M; Muramatsu Y; Ishii MM; Miyakoshi S; Takatsu T; Inukai M; Kakuta M; Abe T; Harasaki T; Fukuoka T; Utsui Y; Ohya S Synthesis and antimycobacterial activity of capuramycin analogues. Part 1: substitution of the azepan-2-one moiety of capuramycin. Bioorg. Med. Chem. Lett 2003, 13, 2829–2832. [PubMed: 14611838]

(53). Knapp S; Nandan SR Synthesis of capuramycin. J. Org. Chem 1994, 59, 281–283.

(54). Wang Q; Wang Y; Kurosu M A new Oxyma derivative for nonracemizable amide-forming reactions in water. Org. Lett 2012, 14, 3372–3375. [PubMed: 22697488]

(55). Dery M-A; Jodoin J; Ursini-Siegel J; Aleynikova O; Ferrario C; Hassan S; Basik M; LeBlanc AC Endoplasmic reticulum stress induces PRNP prion protein gene expression in breast cancer. Breast Cancer Res 2013, 15, R22. [PubMed: 23497519]

(56). Banerjee A; Lang J-Y; Hung M-C; Sengupta K; Banerjee SK; Baksi K; Banerjee DK Unfolded protein response is required in nu/nu mice microvasculature for treating breast tumor with tunicamycin. J. Biol. Chem 2011, 286, 29127–29138. [PubMed: 21676868]

(57). https://www.proteinatlas.org/ENSG00000172269-DPAGT1/tissue

(58). Grzegorzewicz AE; Ma YE; Jones V; Crick DC; Liav A; McNeil MR Development of a microtitre plate-based assay for lipid-linked glycosyltransferase products using the mycobacterial cell wall rhamnosyltransferase WbbL, Microbiology 2008, 154, 3724–3730. [PubMed: 19047740]

(59). Mitachi K; Yun H-G; Gillman CD; Skorupinska-Tudek K; Swiezewska E; Clemons WM; Kurosu M Substrate tolerance of bacterial glycosyltransferase MurG: Novel fluorescence-based assays. ACS Infect. Dis 2019 Accepted for publication. 10.1021/acsinfecdis.9b00242

(60). Greenwood JR; Calkins D; Sullivan AP; Shelley JC Towards the comprehensive, rapid, and accurate prediction of the favorable tautomeric states of drug-like molecules in aqueous solution. J. Comput. Aided Mol. Des 2010, 24, 591–604. [PubMed: 20354892]

(61). Friesner RA; Banks JL; Murphy RB; Halgren TA; Klicic JJ; Mainz DT; Repasky MP; Knoll EH; Shelley M; Perry JK; Shaw DE; Francis P; Shenkin PS Glide: a new approach for rapid, accurate docking and scoring. 1. Method and assessment of docking accuracy. J. Med. Chem 2004, 25, 1739–1749.

(62). Friesner RA; Murphy RB; Repasky MP; Frye LL; Greenwood JR; Halgren TA; Sanschagrin PC; Mainz DT Extra precision glide: docking and scoring incorporating a model of hydrophobic enclosure for protein-ligand complexes. J. Med. Chem 2006, 49, 6177–6196. [PubMed: 17034125]

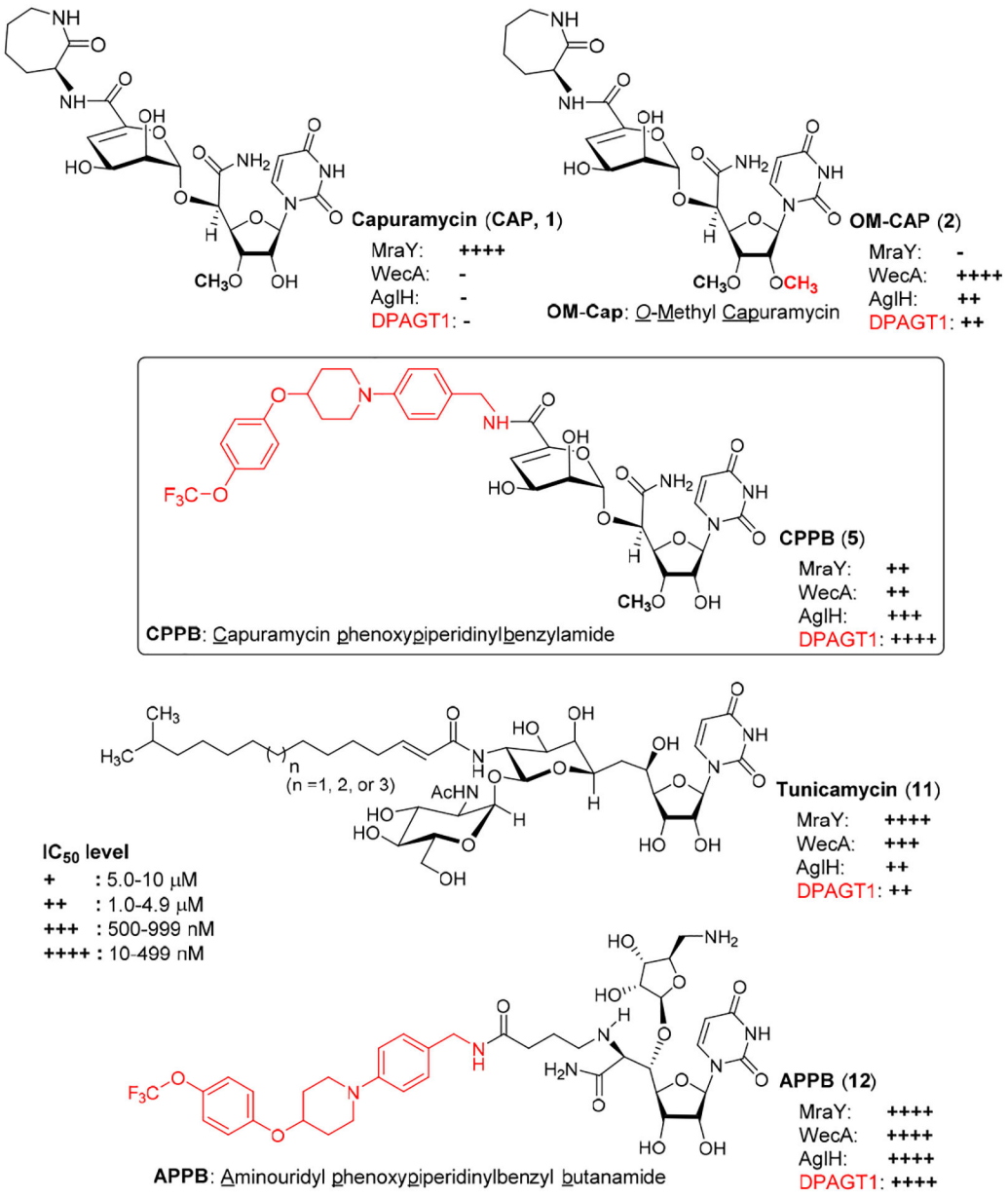

Figure 1.

Development of DPAGT1 Inhibitors of Capuramycin Analogues. Structures of Capuramcyin, *O*-Methyl capuramycin (OM-Cap), Capuramycin phenoxypiperidinylbenzylamide analogue (CPPB), Aminouridyl phenoxylpiperidinylbenzylbutanamide (APPB, Previously Reported DPAGT1 Inhibitor), and Tunicamycin (Reference Molecule).

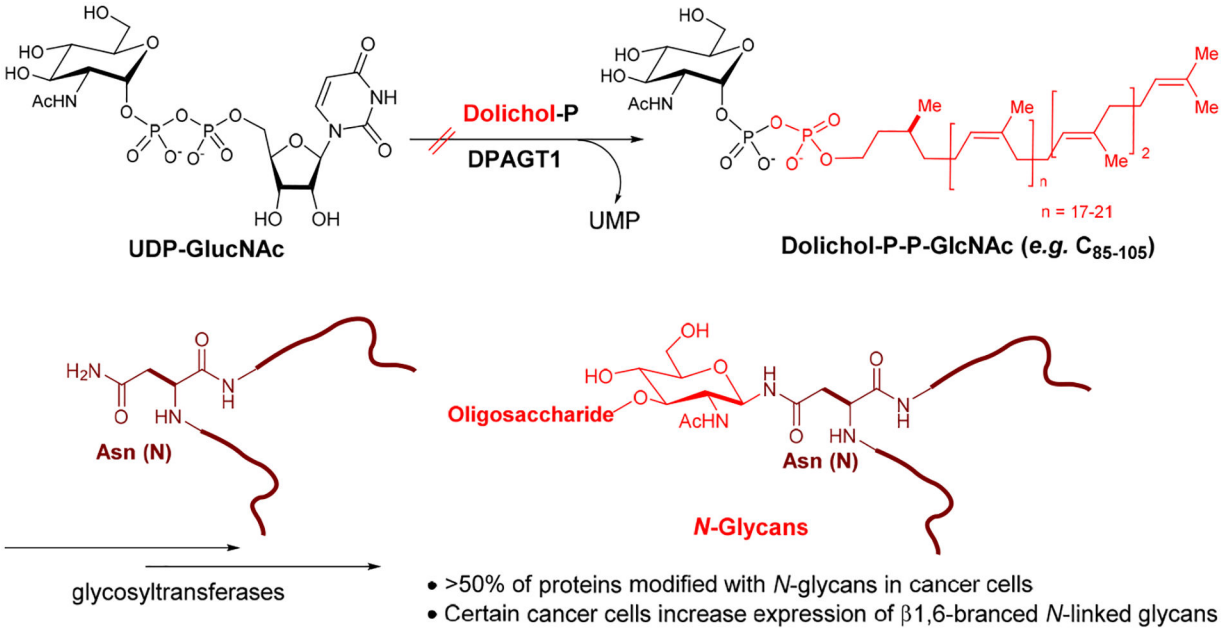

Figure 2.
DPAGT1 in *N*-Glycan Biosynthesis.

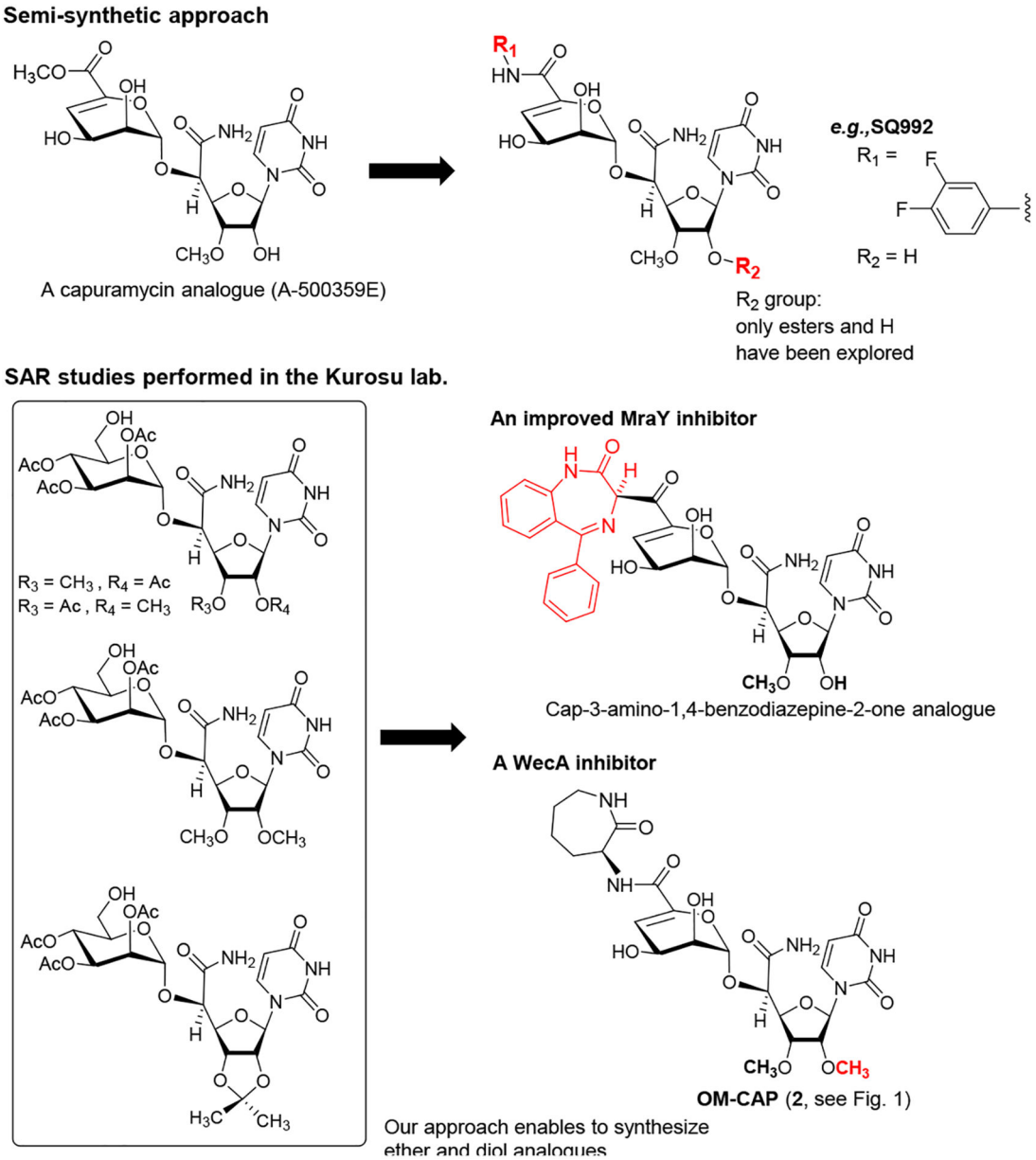

Figure 3.
General Strategy of SAR of Capuramycin.

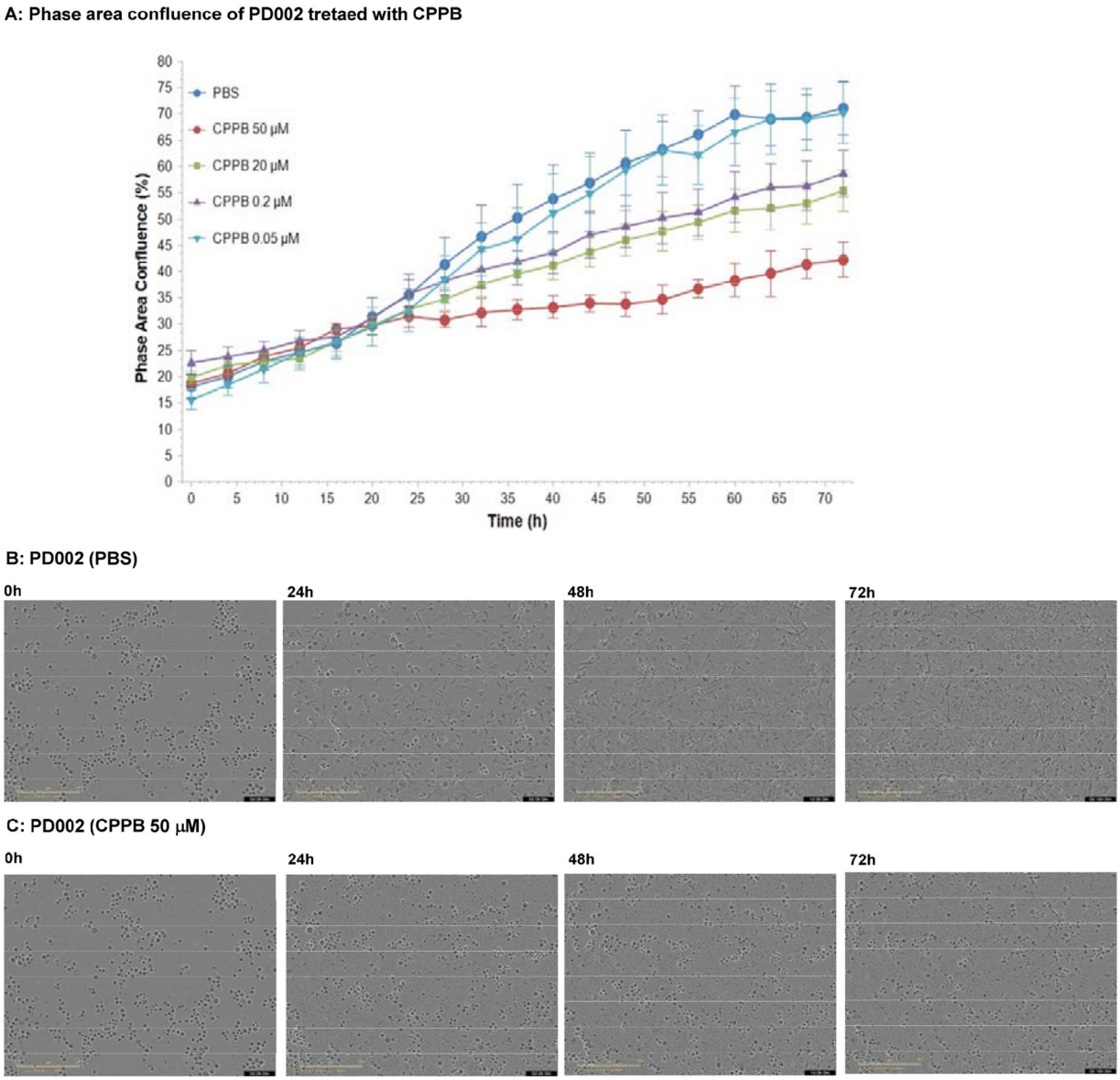

Figure 4.

Kinetic Proliferation Assays for PD002 Treated with CPPB Monitored by IncuCyte® Live Cell Analysis.[a]

[a]Images were obtained every 4h using an IncuCyte Live-Cell Imaging System (Essen BioScience, Ann Arbor, MI). After 72h, cell proliferation was quantified using the metric phase object confluence (POC), the area of the field of view that is covered by cells (phase area confluence %) is calculated by the integrated software.

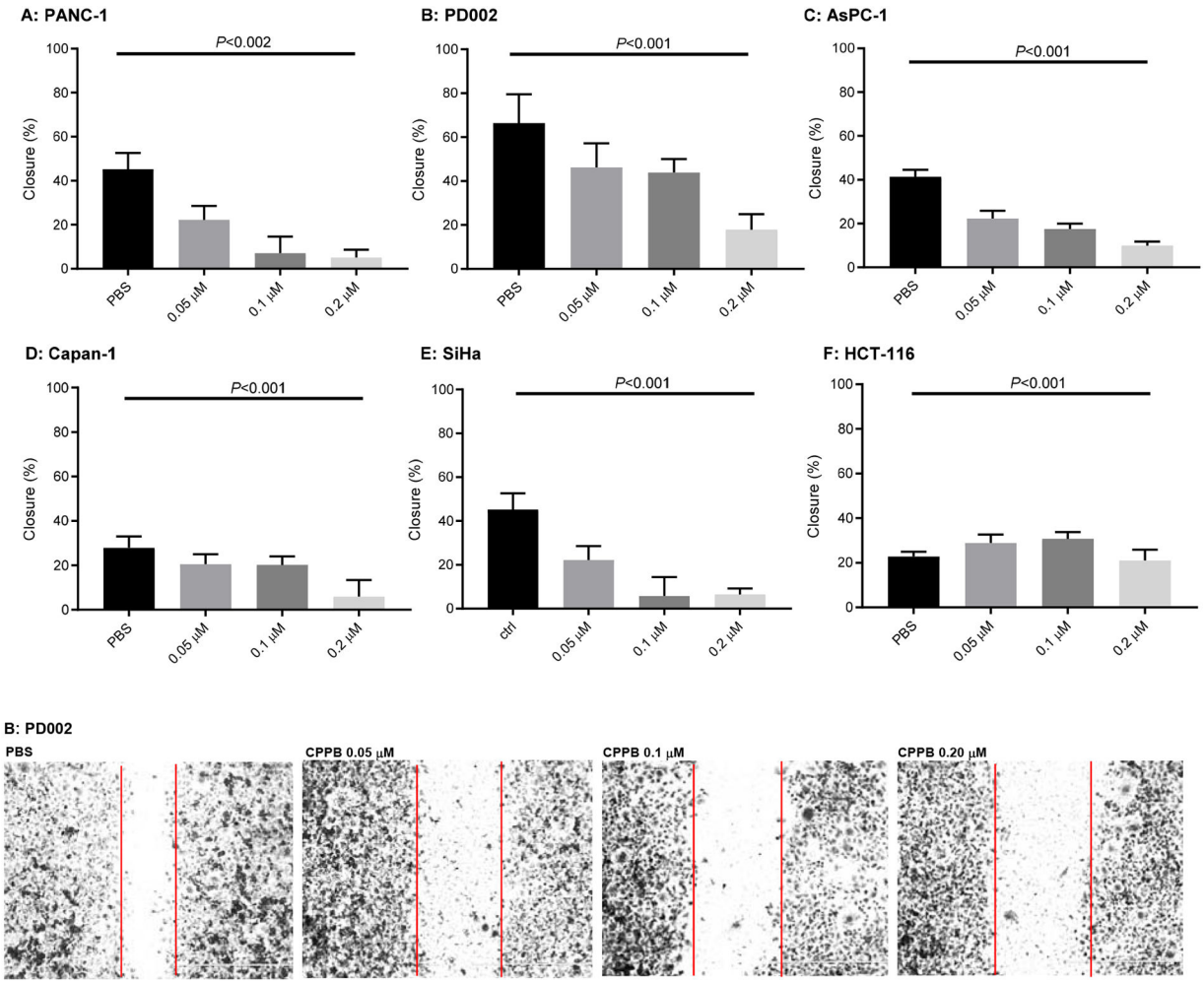

Figure 5.

Analyses of Migration inhibition of Pancreatic Cancers (PANC-1, PD002, AsPC-1, and Capan-1), a Cervical carcinoma (SiHa), a Colorectal Adenocarcinoma (HCT-116) by Treatment with CPPB in Would Healing (Scratch) Assays.[a]

[a]All images were acquired at 24h and these are summarized in SI (only the data for PD002 shown). *P* values were obtained from T score calculator.

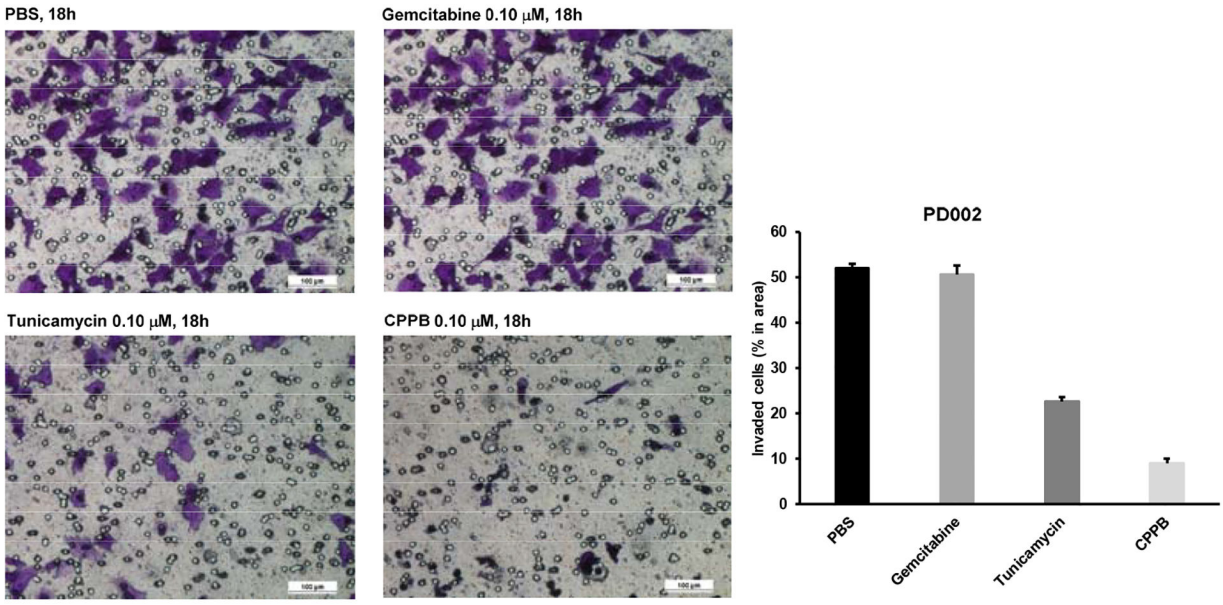

Figure 6.

Cell Migration Inhibition of PD002 by Gemcitabine, Tunicamycin, and CPPB via Transwell Chamber.[a]

[a]The cells were fixed using 4% paraformaldehyde for 0.5h and stained with 0.05% crystal violet (300 μL/well), after 0.5h, the images were captured via 10X magnification microscopy.

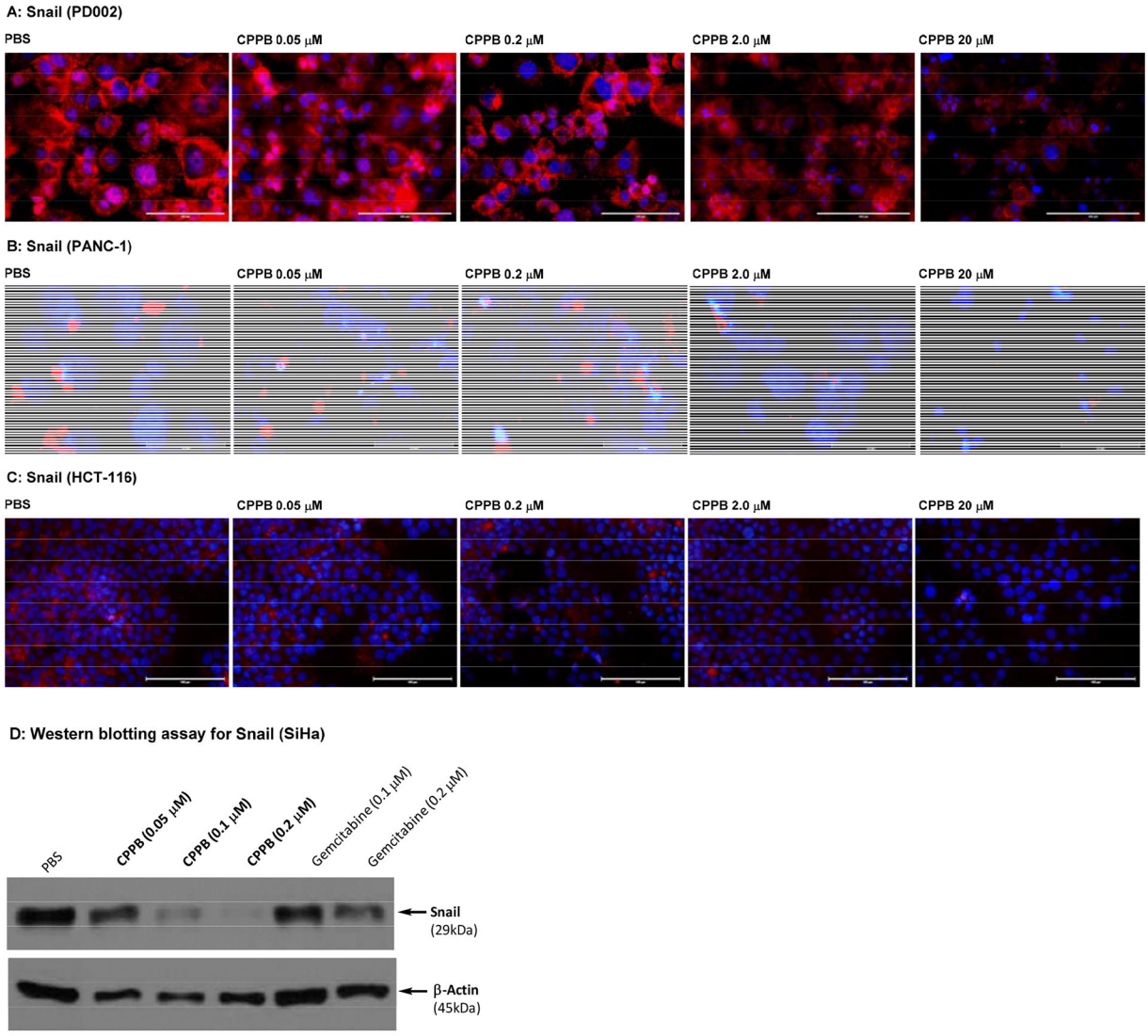

Figure 7.

Immuno-fluorescent staining: Effect of a DPAGT1 Inhibitor, CPPB, on Snail in Pancreatic Cancer Cells (PD002 and PANC-1) and a Colorectal Adenocarcinoma (HCT-116). Western Blotting Assay for a Cervical Cancer (SiHa).[a]

[a]Fluorescence microscopy images at 40x. The cells ($1 \times 10^{5-6}$) were treated with CPPB (0.05, 0.2, 2.0, and 20 μM) or PBS for 24h. For immunefluorescent studies: the cells were treated with Snail (C15D3) rabbit mAb (Cell Signaling Technology), followed by Goat anti-Rabbit IgG (H+L) Cross-Adsorbed Secondary Antibody, Alexa Fluor™568 (red). DAPI (4′,6-diamidino-2-phenylindole), a blue fluorescent DNA dye, was used to mark the nucleus. 40x. For Western blotting assays: The cells were treated with Snail (C15D3) rabbit mAb (Cell Signaling Technology), followed by secondary antibody, horseradish peroxidase (HRP)-linked antibody (Cell Signaling Technology).

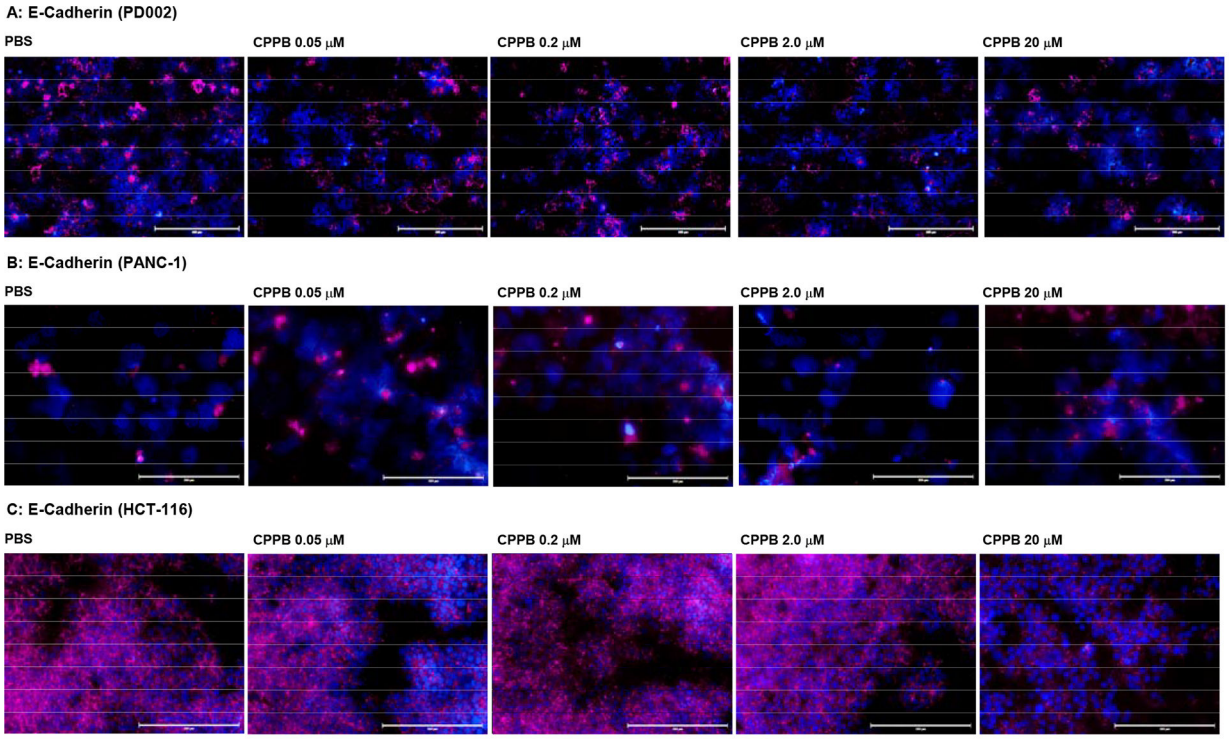

Figure 8.

Immunofluorescent Staining: Effect of a DPAGT1 inhibitor, CPPB, on E-Cadherin in Pancreatic cancer cells (PD002 and PANC-1) and a Colorectal Adenocarcinoma (HCT-116).[a]

[a]Fluorescence microscopy images at 20x. The cells ($1 \times 10^{5-6}$) were treated with CPPB (0.05, 0.2, 2.0, and 20 μM) or PBS for 24h. The cells were treated with E-cadherin (4A2) mouse mAb (Cell Signaling Technology), followed by secondary antibody, goat anti-mouse IgG (H+L), Alexa Fluor™ Plus 647 (Invitrogen). DAPI (4′,6-diamidino-2-phenylindole), a blue fluorescent DNA dye, was used to mark the nucleus. 40x

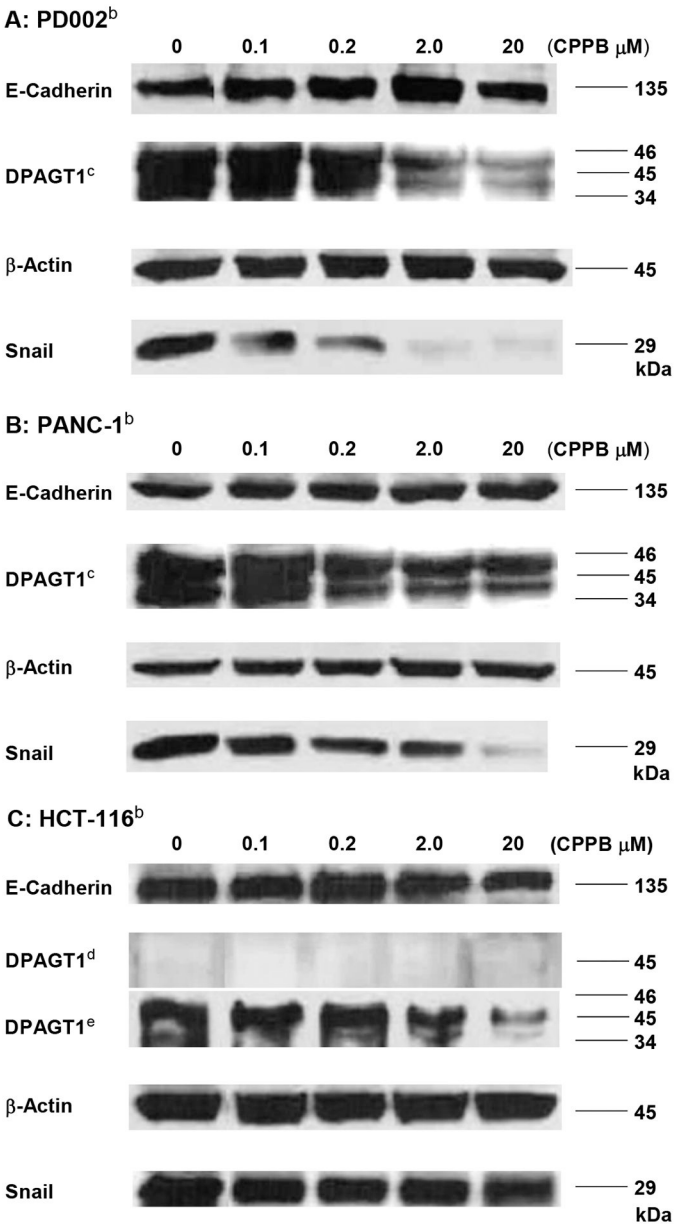

Figure 9.

Western blot Analyses of DPAGT1, Snail, and E-Cadherin in PD002, PANC-1, and HCT-116 treated with CPPB.[a]

[a]The relative expression level was quantified by using Image Studio™ Lite quantification software ($n = 3$, $p<0.001$, see SI).; [b]All cell lysates were prepared to be 1.5 mg total protein/mL by 15,200 xg, 30min at 4 °C unless indicated. [C]At least three isoforms of DPAGT1 were detected.; [d]DPAGT1 was not detectable at 30 μL (1.5 mg total protein /mL).; [e]The cell lysate was prepared by ultracentrifugation (130,000 xg for 1h at 4 °C). 30 μL of the lysate was analyzed.

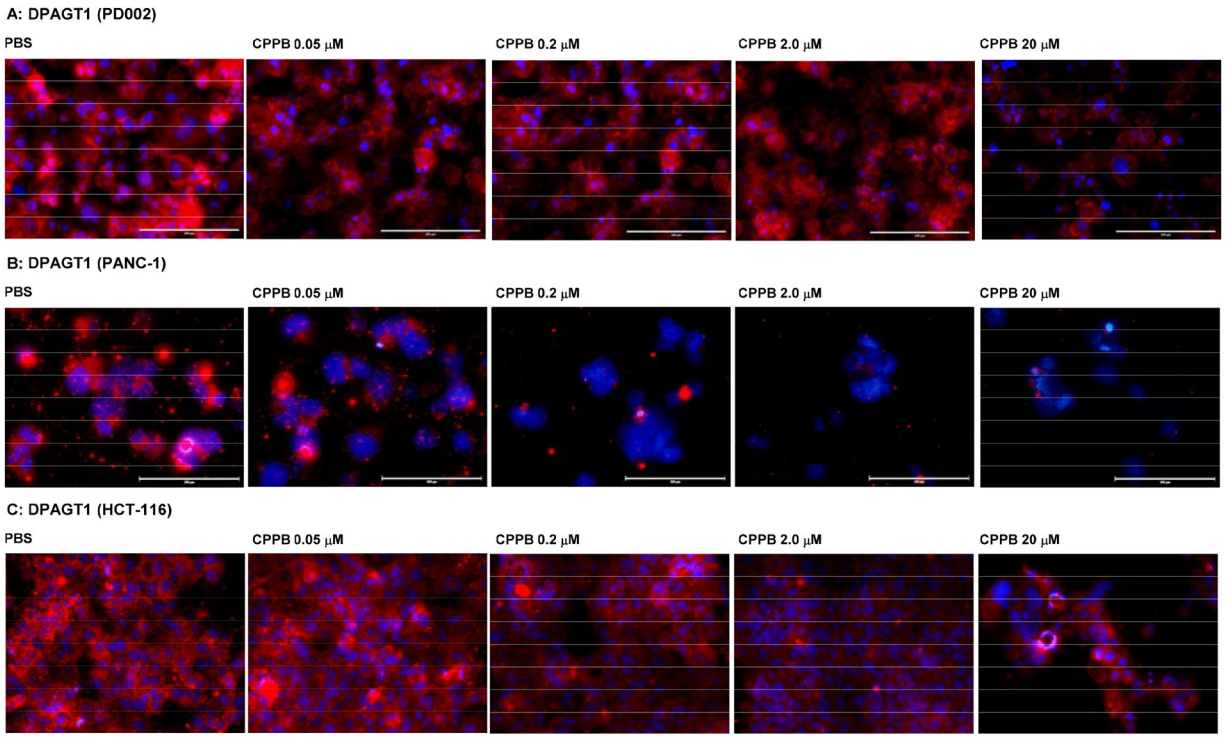

Figure 10.

Immunofluorescent staining: The DPAGT1 Expression Level in the Selected Cancer Cell Lines (PD002 and PANC-1) and a Colorectal Adenocarcinoma (HCT-116) Treated with CPPB.[a]

[a]Fluorescence microscopy images at 20x. The cells ($1 \times 10^{5-6}$) were treated with CPPB (0.05, 0.2, 2.0, and 20 μM) or PBS for 72h. The cells were treated with DPAGT1 polyclonal antibody (Invitrogen, PA5–72704), followed by secondary antibody, Donkey anti-rabbit IgG (H+L), Alexa Fluor™ 555 (red) (Invitrogen). DAPI (4′,6-diamidino-2-phenylindole), a blue fluorescent DNA dye, was used to mark the nucleus.

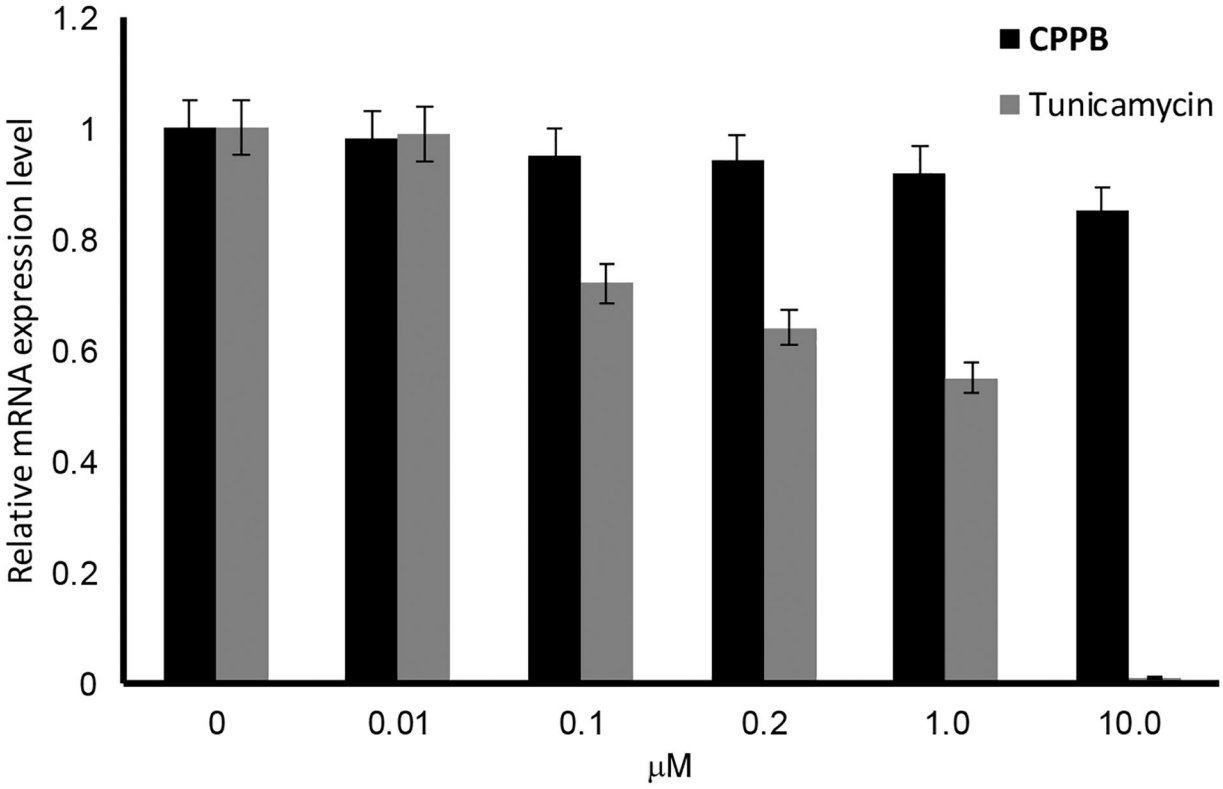

Figure 11.

RT-qPCR Analyses of *DPAGT1* Expression Level in PD002 Treated with CPPB.[a]

[a]~5 ×10^6 of PD002 was applied. Incubation time: 24h at 37 °C. At 10 μM, tunicamycin killed PD002 in 100%.

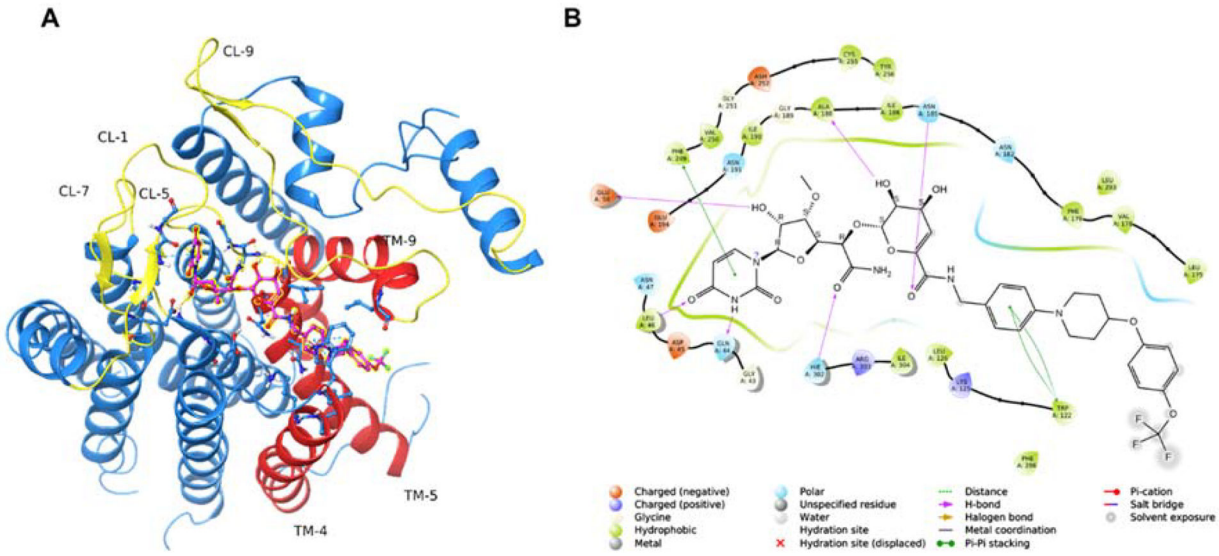

Figure 12.

Modeling CPPB-DPAGT1 Interaction to Design New Inhibitor Molecules.[a]

[a]Docking studies were performed using the human DPAGT1 with bound tunicamycin (PDB: 6BW6) (PMID 29459785). The biological unit was downloaded and prepared using the Protein Preparation Wizard of the Maestro Small Molecule Drug Discovery Suite (Schrödinger, LLC). The docking receptor grid was prepared using Schrödinger's Glide program. (PMID 15027866, PMID 15027865). CPPB was built and prepared for docking using the LigPrep program using default settings (Schrödinger, LLC). **A:** Predicted binding pose of CPPB (highlighted ball & stick model) into DPAGT1. Key active site loops (yellow) and transmembrane regions (orange) are indicated. **B:** 2D ligand interaction diagram of the docked CPPB-DPAGT1 complex with key predicted interactions shown.

CL: cytoplasmic loop.; TM: transmembrane segment

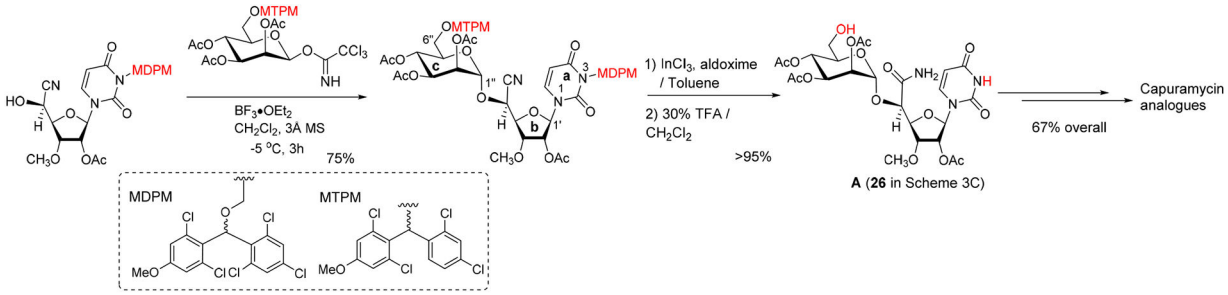

Scheme 1.

An Improved Synthesis of Capuramycin Analogues Developed in The Kurosu Lab.

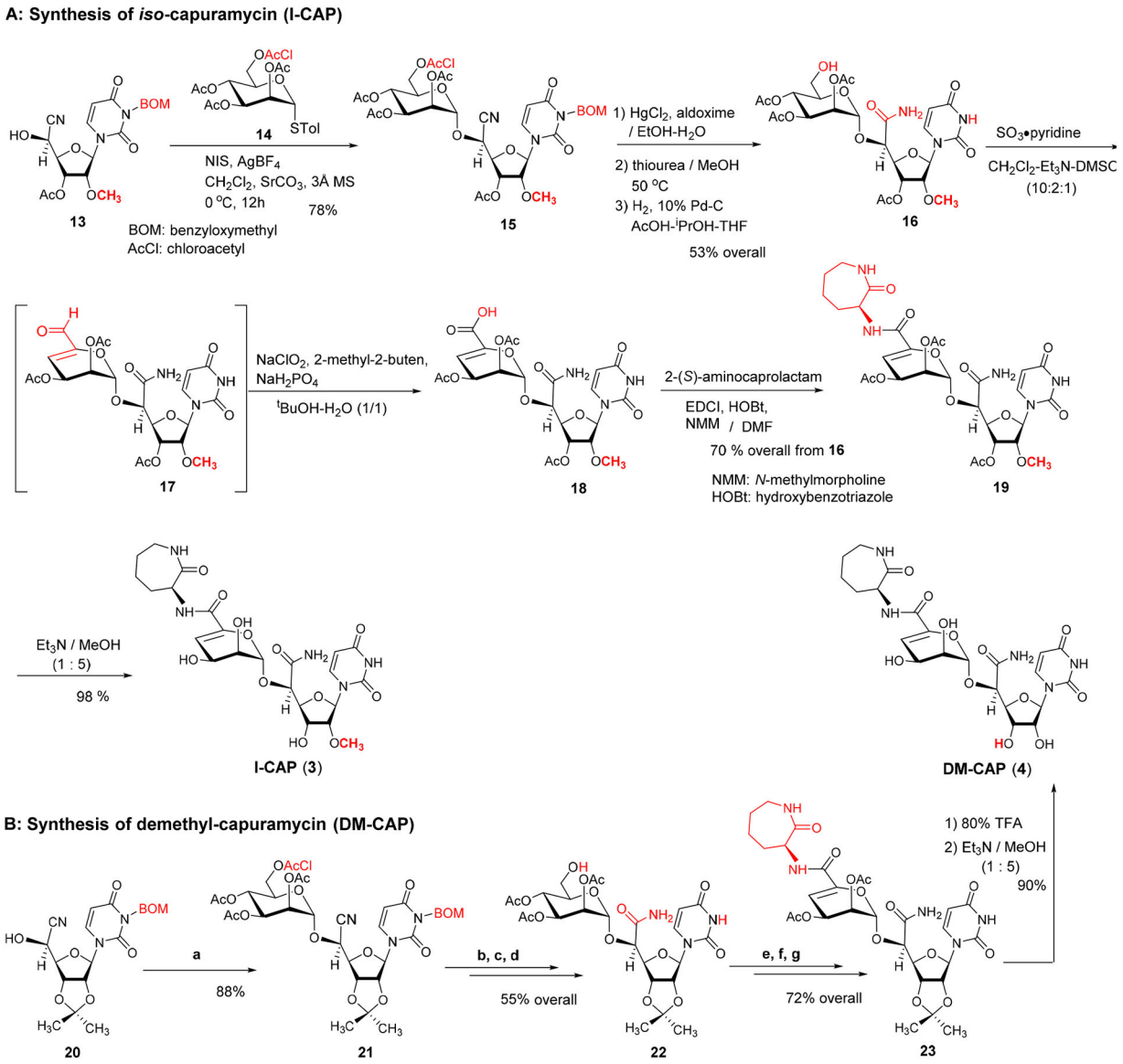

Scheme 2.

Syntheses of *iso*-Capuramycin (I-CAP, 3) and Demethyl-capuramycin (DM-CAP, 4).

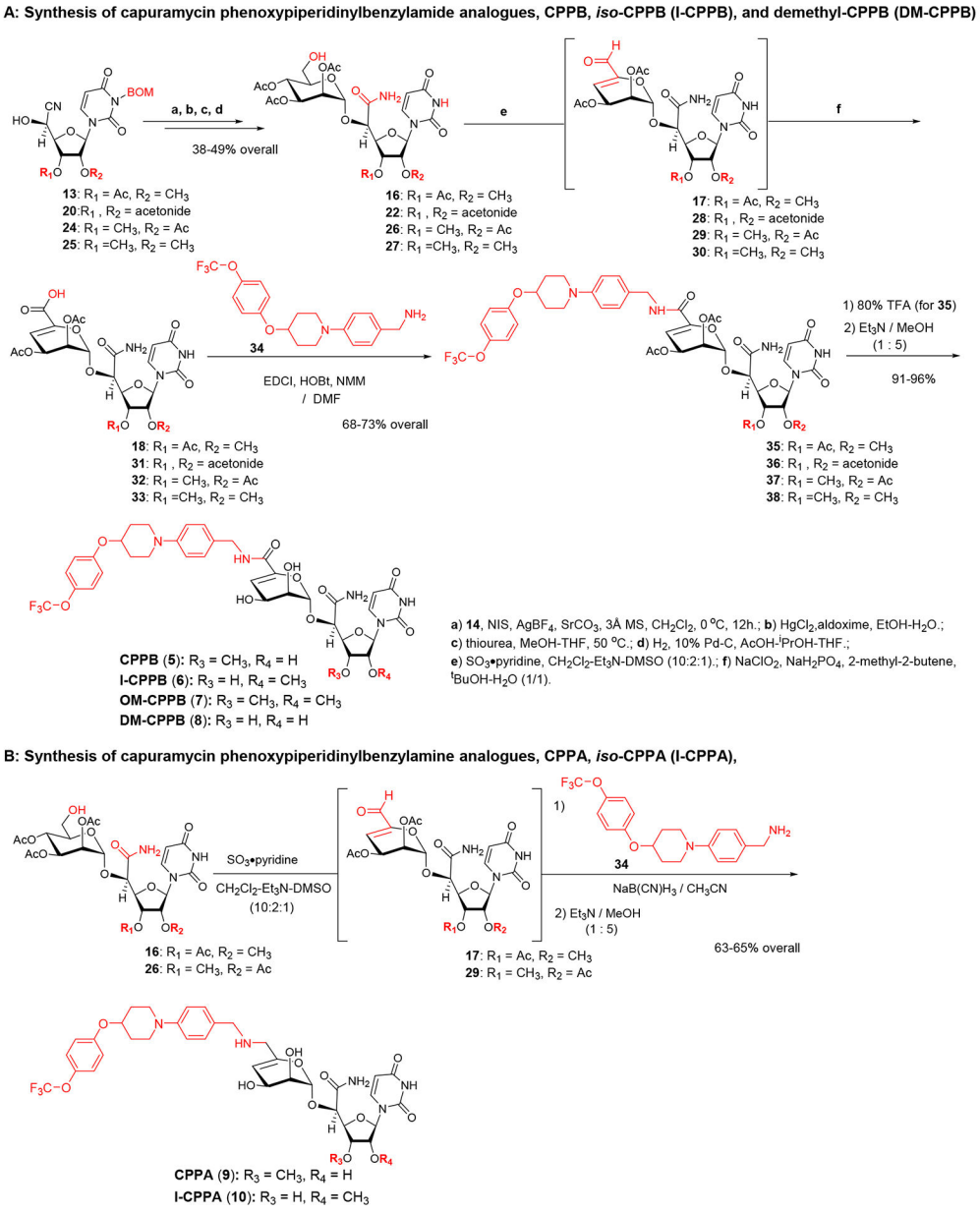

Scheme 3.

Syntheses of Capuramycin phenoxypiperidinylbenzylamine (CPPA, **9**) and *iso*-Capuramycin phenoxypiperidinylbenzylamine (I-CPPA, **10**).

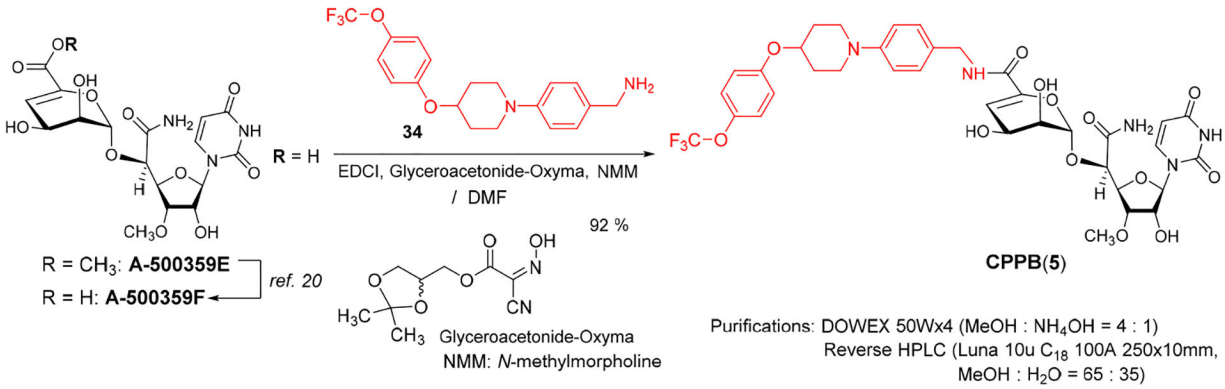

Scheme 4.

A Semi-synthesis of CPPB from Synthetic A-500359F, a Metabolite of *S. griseus* SANK60196.

Table 1.

Phosphotransferase Enzyme Inhibitory Activities of Capuramycin Analogues.[a]

Entry	Compound	IC_{50} (μM)[a]			
		MraY (*Hydrogenivirga sp.*)	**WecA (*E. coli*)**	**AglH (*M. jannaschii*)**	**DPAGT1 (Human)**
1	Capuramycin (CAP, **1**)	0.13	>50	>50	>50
2	*O*-Methyl capuramycin (OM-CAP, **2**)	>50	0.060	2.5	4.5
3	*iso*-Capuramycin (I-CAP, **3**)	8.5	30.0	20.0	11.5
4	Demethyl capuramycin (DM-CAP, **4**)	>50	35.0	>50	>50
5	Capuramycin phenoxypiperidinylbenzylamide (CPPB, **5**)	10.3	0.10	0.15	0.20
6	*iso*-Capuramycin phenoxypiperidinylbenzylamide (I-CPPB, **6**)	>50	20.0	15.0	0.60
7	*O*-Methyl capuramycin phenoxypiperidinylbenzylamide (OM-CPPB, **7**)	5.0	10.0	30.0	20.0
8	Demethyl capuramycin phenoxypiperidinylbenzylamide (DM-CPPB, **8**)	>50	30.0	>50	>50
9	Capuramycin phenoxypiperidinylbenzylamine (CPPA, **9**)	>50	>50	>50	>50
10	*iso*-Capuramycin phenoxypiperidinylbenzylamine (I-CPPA, **10**)	>50	>50	>50	>50
11	Tunicamycin (**11**)	2.9	0.15	13.2	1.5

[a]All assay protocols are summarized in Experimental Section as well as SI.

Table 2.

Cytotoxicity of Capuramycin, Capuramycin Analogues, and Tunicamycin.

Entry	Compound	IC_{50} (μM)[a]										
L1210	KB	SiHa	HCT-116	DLD-1	Capan-1	PANC-1	AsPC-1	PD002	HPNE	Vero		
1	CAP (**1**)	>50	>50	>50	>50	>50	>50	>50	>50	>50	>50	>50
2	OM-CAP (**2**)	>50	>50	>50	>50	>50	>50	>50	>50	>50	>50	>50
3	CPPB (**5**)	>50	35.0	15.0	15.0	25.0	30.0	35.0	25.0	35.0	>50	>50
4	I-CPPB (**6**)	>50	35.0	25.0	25.0	35.0	40.0	45.0	30.0	50.0	>50	>50
5	Tunicamycin (**11**)	1.70	2.50	0.92	0.92	1.25	1.50	1.50	0.45	1.50	7.5	0.78

CAP: Capuramycin.; OM-CAP: *O*-Methyl capuramycin.; CPPB: Capuramycin phenoxypiperidinylbenzylamide.; I-CCB: *iso*-Capuramycin phenoxypiperidinylbenzylamide.; L1210 (ATCC® CCL-219™): mouse lymphocytic leukemia.; KB (ATCC® CCL-17™): HeLa, human cervical carcinoma.; SiHa (ATCC® HTB-35™): human cervical squamous cell carcinoma.; HCT-116 (ATCC® CCL-247™): colorectal adenocarcinoma.; DLD-1 (ATCC® CCL221™): colorectal adenocarcinoma.; Capan-1 (ATCC® HTB-79™): pancreatic ductal adenocarcinoma.; PANC-1 (ATCC® CRL-1469™): pancreatic ductal carcinoma.; AsPC-1 (ATCC® CRL-1682™): pancreatic adenocarcinoma.; PD002: a pancreatic adenocarcinoma staged at T3N1M0 from a 55 years old Caucasian male in 2011 (provided by Dr. Glazer (University of Tennessee Health Science Center).; hTERT-HPNE (ATCC® CRL-4023™): normal pancreatic ductal cell.; Vero (ATCC® CCL-81™): normal Cercopithecus aethiops kidney cell.

[a] IC_{50} values were determined via MTT assay.

Table 3.

Fractional Inhibitory Concentration (FIC) of a Combination of CPPB and Paclitaxel against a Patient-derived Pancreatic Adenocarcinoma PD002.[a]

Entry	Combination of A and B[b]	C_A and C_B (μM)[c]	ΣFIC[d]
1	A: CPPB	0.10	0.50
	B: Paclitaxel	0.63	
2	A: CPPB	0.10	0.13
	B: Paclitaxel	0.16	
3	A: CPPB	0.20	0.0096
	B: Paclitaxel	0.0049	
4	A: CPPB	0.20	0.021
	B: Paclitaxel	0.020	
5	A: CPPB	0.20	0.26
	B: Paclitaxel	0.031	
6	A: CPPB	2.0	0.021
	B: Paclitaxel	0.020	
7	A: CPPB	2.0	0.037
	B: Paclitaxel	0.039	
8	A: CPPB	2.0	0.26
	B: Paclitaxel	0.31	

[a] ΣFIC index for the wells at growth–no growth interface.

[b] The IC_{50} values of CPPB and paclitaxel against PD002 are 35.0 and 1.25 μM, respectively.

[c] C_A and C_B are concentrations of A and B.

[d] ΣFIC is the sum of fractional inhibitory concentration calculated by the equation $\Sigma FIC = FIC_A + FIC_B = C_A/IC_{50A} + C_B/IC_{50B}$. Cellular behavior of PD002 treated with paclitaxel or a combination with paclitaxel and CPPB was monitored over time by IncuCyte® live cell analysis (Supporting Information).